NAVAL
POSTGRADUATE
SCHOOL

MONTEREY, CALIFORNIA

THESIS

SOLID HYDROCARBON ASSISTED REDUCTION: A NEW PROCESS OF GENERATING MICRON SCALE METAL PARTICLES

by

Ryan M. McCabe

March 2015

Thesis Advisor:	Jonathan Phillips
Co-Advisor:	Claudia Luhrs

Approved for public release; distribution is unlimited

THIS PAGE INTENTIONALLY LEFT BLANK

REPORT DOCUMENTATION PAGE

Form Approved OMB No. 0704-0188

Public reporting burden for this collection of information is estimated to average 1 hour per response, including the time for reviewing instruction, searching existing data sources, gathering and maintaining the data needed, and completing and reviewing the collection of information. Send comments regarding this burden estimate or any other aspect of this collection of information, including suggestions for reducing this burden, to Washington headquarters Services, Directorate for Information Operations and Reports, 1215 Jefferson Davis Highway, Suite 1204, Arlington, VA 22202-4302, and to the Office of Management and Budget, Paperwork Reduction Project (0704-0188) Washington DC 20503.

1. AGENCY USE ONLY *(Leave blank)*	2. REPORT DATE March 2015	3. REPORT TYPE AND DATES COVERED Master's Thesis	
4. TITLE AND SUBTITLE SOLID HYDROCARBON ASSISTED REDUCTION: A NEW PROCESS OF GENERATING MICRON SCALE METAL PARTICLES		**5. FUNDING NUMBERS**	
6. AUTHOR(S) Ryan M. McCabe			
7. PERFORMING ORGANIZATION NAME(S) AND ADDRESS(ES) Naval Postgraduate School Monterey, CA 93943-5000		**8. PERFORMING ORGANIZATION REPORT NUMBER**	
9. SPONSORING /MONITORING AGENCY NAME(S) AND ADDRESS(ES) N/A		**10. SPONSORING/MONITORING AGENCY REPORT NUMBER**	

11. SUPPLEMENTARY NOTES The views expressed in this thesis are those of the author and do not reflect the official policy or position of the Department of Defense or the U.S. Government. IRB Protocol number ____N/A____.

12a. DISTRIBUTION / AVAILABILITY STATEMENT Approved for public release; distribution is unlimited	12b. DISTRIBUTION CODE

13. ABSTRACT (maximum 200 words)

The goal of this research is to test a central hypothesis: that gas species generated by the thermal and/or catalytically assisted decomposition of hydrocarbons in an inert atmosphere can reduce metal oxides to a metallic state. It is postulated that the decomposition releases gas phase radicals that can bind with oxygen in the metal oxides, forming volatile, stable oxides such as CO_2 and water. This research consisted of thermally decomposing several types of solid hydrocarbon, including wax and low-grade coal, both with and without catalysts, in a nitrogen environment at >600 °C, located immediately below beds of micron scale particles of either NiO or Fe_3O_4. X-ray diffraction and scanning electron microscopy analysis showed, in support of the hypothesis, both metal oxides reduced to some extent. Nickel oxide reduced fully in many cases, but iron oxide never fully reduced and the extent of reduction was found to be a function of hydrocarbon, catalyst and temperature. These results suggest solid hydrocarbon assisted reduction (SHAR) with further testing and development may be a practical means to make sub-micron particles suitable in terms of price and quality for use in particle injection molding and 3D manufacturing of precision metal parts.

14. SUBJECT TERMS SHAR, Reduction, Nanoparticles, Additive Manufacturing, 3D Printing			15. NUMBER OF PAGES 91
			16. PRICE CODE
17. SECURITY CLASSIFICATION OF REPORT Unclassified	**18. SECURITY CLASSIFICATION OF THIS PAGE** Unclassified	**19. SECURITY CLASSIFICATION OF ABSTRACT** Unclassified	**20. LIMITATION OF ABSTRACT** UU

NSN 7540-01-280-5500

Standard Form 298 (Rev. 2-89)
Prescribed by ANSI Std. 239-18

THIS PAGE INTENTIONALLY LEFT BLANK

SOLID HYDROCARBON ASSISTED REDUCTION: A NEW PROCESS OF GENERATING MICRON SCALE METAL PARTICLES

Ryan M. McCabe
Lieutenant, United States Navy
B.S., University of New Mexico, 2008

Submitted in partial fulfillment of the
requirements for the degree of

MASTER OF SCIENCE IN MECHANICAL ENGINEERING

from the

**NAVAL POSTGRADUATE SCHOOL
March 2015**

Author: Ryan M. McCabe

Approved by: Jonathan Phillips
         Thesis Advisor

         Claudia Luhrs
         Thesis Co-Advisor

         Garth V. Hobson
         Chair, Department of Mechanical and Aerospace
         Engineering

THIS PAGE INTENTIONALLY LEFT BLANK

ABSTRACT

The goal of this research is to test a central hypothesis: that gas species generated by the thermal and/or catalytically assisted decomposition of hydrocarbons in an inert atmosphere can reduce metal oxides to a metallic state. It is postulated that the decomposition releases gas phase radicals that can bind with oxygen in the metal oxides, forming volatile, stable oxides such as CO_2 and water. This research consisted of thermally decomposing several types of solid hydrocarbon, including wax and low-grade coal, both with and without catalysts, in a nitrogen environment at >600 °C, located immediately below beds of micron scale particles of either NiO or F_e3O_4. X-ray diffraction and scanning electron microscopy analysis showed, in support of the hypothesis, both metal oxides reduced to some extent. Nickel oxide reduced fully in many cases, but iron oxide never fully reduced and the extent of reduction was found to be a function of hydrocarbon, catalyst and temperature. These results suggest solid hydrocarbon assisted reduction (SHAR) with further testing and development may be a practical means to make sub-micron particles suitable in terms of price and quality for use in particle injection molding and 3D manufacturing of precision metal parts.

THIS PAGE INTENTIONALLY LEFT BLANK

TABLE OF CONTENTS

LIST OF FIGURES

THIS PAGE INTENTIONALLY LEFT BLANK

LIST OF TABLES

THIS PAGE INTENTIONALLY LEFT BLANK

LIST OF ACRONYMS AND ABBREVIATIONS

Å	angstrom
ang	angstrom
Ar	argon
BSE	back scatter electron
C	degrees Celsius
$CaCO_3$	calcium carbonate
cc	cubic centimeter
cm	centimeter
CO_2	carbon dioxide
CO	carbon monoxide
CRT	cathode ray tube
deg	degree
EDAX	energy dispersive analysis of x-rays
EDS	energy dispersive x-ray spectroscopy
Fe	iron
FeO	wustite
Fe_2O_3	iron (II) oxide
Fe_3O_4	magnetite
g	gram
H_2	hydrogen
H_2O	water
K_2CO_3	potassium carbonate
kg	kilogram
kcal	kilocalorie
kW	kilowatt
m	meter
min	minute
mol	mole
μm	micron
NDR	no data recorded

$Na_2CO_3\ H_2O$	sodium carbonate monohydrate
Ni	nickel
NiO	nickel oxide
Nm	nanometer
PIM	particle injection molding
SEM	scanning electron microscope
SHAR	solid hydrocarbon assisted reduction
XRD	x-ray diffraction

ACKNOWLEDGMENTS

THIS PAGE INTENTIONALLY LEFT BLANK

I. INTRODUCTION

3D manufacturing is a method of intense interest to both the U.S. government, and industrial firms world wide [1]. The Navy is interested in the use of 3D manufacturing as a means to reduce the tonnage of spare parts required on vessels. As only a small fraction of stored parts are employed in any single voyage, most of the spare part tonnage is an expensive (space and cost), complex, insurance policy. The hope is that instead of carrying parts, the vessels will take "software instructions", a "3D printer" and the raw material required for the construction process. This will reduce storage space, inventory management, supplier complexity and capital cost. In some ways, the switch from spare part inventories to 3D manufacturing can be compared to the dramatic cost reduction associated with a switch for major manufacturing processes from storing parts to just-in-time protocols.

One major barrier to implementing this technology is that at present it works well only for plastic-based parts. Metal printer technology is more complex and expensive and the raw material, metal particles, is also expensive. Some of these technological barriers are gradually being overcome. In particular, the quality and reliability of 3D metal manufacturing tools is constantly improving, while capital investment requirements for equipment are expected to continue current downward trends [2]. Yet, it is not clear that there has been any similar improvement in the quality and cost of metal particles.

The cost of particles is associated with the additional steps involved in the manufacturing technique. For example, to produce iron particles the first step is to produce bulk iron using the standard blast furnace approach. Iron particles are inherently more expensive than bulk iron because particle production requires an additional step. Metallic iron in molten form must be forced at high pressure through a nozzle or sieve under reducing conditions. The molten iron streams generated in this fashion break up, forming particles, which are subsequently solidified in a rapid cooling process. This technique, known as atomization, has

other limits as well. Indeed, the name is a misnomer. The particles that form are not particularly small. Average particle size is of the order of 50 microns. This actually limits the size of features that can be produced with the particles. Indeed, a smooth, full strength, part made from sintered particles requires that the particles be no more than ~10% of the size of the feature. To some extent the smaller particles in the distribution formed via atomization can be culled. Still, creating particle size distributions in which the average particle size is less than 20 microns is very expensive. Other technologies are available for making smaller particles, such as precipitation from solution, but particles produced in this fashion are prohibitively expensive for bulk manufacturing. Hence, the smallest practical, full strength, features that can realistically be formed using todays' standard, relatively inexpensive, particle technology are about 200 microns in size.

The present work explores a specific alternative to atomization as a means of particle production. In brief, the hypothesis is that reducing radicals produced by heating solid hydrocarbons, including coal, in inert atmospheres can reduce metal oxides. Prior to the present work, this technology was never postulated and never tested. Thus, this thesis presents the testing of a new method for metal particle production. The hypothesis is given this name: Solid Hydrocarbon Assisted Reduction (SHAR).

For the purposes of the initial testing of the SHAR hypothesis as carried out in this thesis, two reactors were staged very closely together, with a separation of no less than 1 millimeter and no more than one centimeter. In one, a source of hydrocarbon was contained. In the other, a metal oxide was placed. With this arrangement, a more specific form of the hypothesis could be tested. To wit: The SHAR hypothesis would be considered validated if the metal oxide was reduced following heating of the two reactors in an inert atmosphere to a temperature sufficient to produce radicals. Other aspects of the SHAR hypothesis were also tested.

- Can SHAR be conducted at a temperature far lower than that required to melt the solid?
- Can micron and even submicron particles be directly produced from metal oxide?
- Can it be demonstrated that SHAR is less expensive than alternative particle production technologies?

The simplest summary of the results is that the SHAR hypothesis has been demonstrated. Specifically:

- SHAR can produce some metal from metal oxides at temperatures far below the melting temperature of the metal.
- Sub-micron metal particles can be produced directly from metal oxide using SHAR.
- SHAR can be successfully carried out using relatively small amounts of lignite coal, a very inexpensive form of solid hydrocarbon suggesting it is indeed a very inexpensive technology.

The work also revealed limitations and clear directions for future work. Although SHAR could fully reduce NiO to form sub-micron Ni metal particles at 850 C, far below the melting temperature of Ni, in this first work we were only able to partially reduce Fe_3O_4 to metallic iron particles, even at 950 C.

There is clearly a need for more work to improve the process, specifically for the reduction of iron ore. The operating temperature may be refined based on the identity of the hydrocarbon and catalyst employed. The physical orientation of the experiment may be altered to ensure a more direct interaction between the oxide particles and the hydrocarbon decomposition products. The treatment time may be the variable of focus for future research, as the decomposition of hydrocarbons is this experiment may prove to be incomplete.

THIS PAGE INTENTIONALLY LEFT BLANK

II. BACKGROUND

To illustrate the potential value of the SHAR technique, the application and potential alternatives must first be evaluated.

A. THREE DIMENSIONAL PRINTING

Three-dimensional printing is of great interest to the Navy, and to the manufacturing industry at large. The U.S. Navy employed the first shipboard 3D printer on USS ESSEX, LHD-2, in the spring of 2014 [3]. Many suggestions for its employment have come for Sailors. For example, big deck ships such as LHDs and CVNs use a miniaturized facsimile of the flight deck colloquially known as an "Ouija Board" that uses models of aircraft to test aircraft staging strategies. A set of these models can range in cost between $8,000 and $10,000, but a version that is manufactured via 3D printing is an order of magnitude more cost effective at a range of $300-$400. [4]

Though this example is useful to illustrate the cost saving opportunity that 3D printing presents, the existing naval applications are limited to the use of polymers. The more ambitious goal is the manufacturing of components out of metal and metal alloys. The ability to construct such components as needed would dramatically relieve the strain on the existing supply system, and would reduce the costly insurance policy that is the soring of spare parts on naval vessels. Any effort that reduces the space required for storage opens the possibility to repurpose space for critical war fighting equipment such as sensors and armament. There are cases in the submarine force where 3D printing has been used to produce parts no longer produced by the original equipment manufacturer [5], which directly impacts fleet readiness.

Improvements in the polymer-based additive manufacturing process are being adapted to metal based methods, but little has been done to improve the quality or production of the raw materials they require. One issue of quality relates to the available metal particle sizes. Metal particles less than ca. 30

microns are very expensive as they represent a very small fraction of the particles produced by grinding or atomization. As the ultimate size of a feature that can be produced using 3D metal printing, with accuracy, strength and smooth finish, is of the order 10 X the dimensions of the particles employed, the current available feedstock limits quality feature size to about 300 micron. The focus of this study is on improving the process to produce reduced metal powders, as would be employed in 3D printing, particularly particle size.

In addition to 3D printing another older, widely used technology based on metal particles is particle injection molding (PIM). This technology allows metal parts to be made from particles injected with wax, or other removable binding material, into molds [6]. The wax is removed by heating or volatilization via pyrolysis, leaving a solid metal part of precise dimensions. Particularly for metal parts with fine components this can lead to tremendous cost savings relative to machining parts. This method is used extensively in the automotive sector, consumer electronics industry, and in the medical field [7]. Similar to 3D printing, the ultimate limitation on the feature size of component is a function of the size of the particles of construction [8]. Although this is not a technology that the Navy is exploring, it indirectly benefits from the existence of the technology. Clearly, Navy vehicles and other items normally include PIM made parts.

B.   INDUSTRIAL ORE REDUCTION

The acceptance of this technique is dependent on its favorability compared to existing metal particle production processes currently in use in industry. In fact, the general process requires two steps. In the first, a very large-scale (tons/hr) continuous process, the iconic pyrometallurgical reduction of iron oxide via blast furnace, is employed to reduce ore to the metallic form. Next, a second process of atomization is employed to convert molten metal into particles. The cost and complexity of this two-step process is outlined below.

1. Blast Furnace

Up to 10,000 tons of product iron can be produced daily in an industrial blast furnace such as the one detailed in Figure 1. These furnaces can exceed 60 m in height and 14 m in diameter [9].
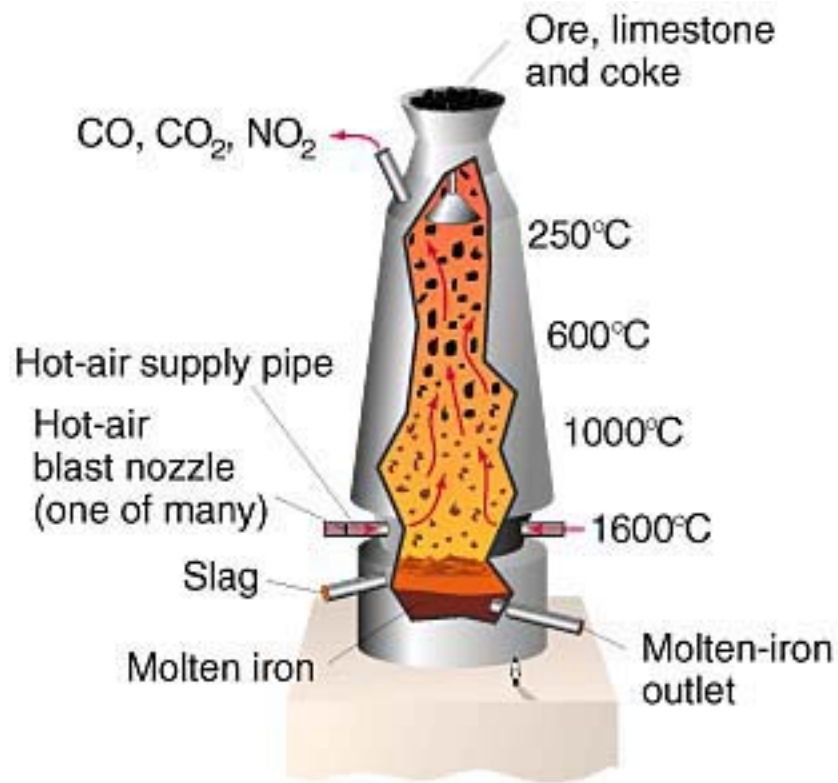
Figure 1.   Blast Furnace for Industrial Iron Ore Reduction
with Figure of a Person for Scale, from [9].

The top of the blast furnace is charged via conveyor with iron, limestone, and coke. Limestone ($CaCO_3$) is used as a source of calcium oxide, which acts as flux to create a fusible slag from silicates and other impurities found in the iron ore [10] by Equation 1. In addition to silica, the slag also contains calcium and magnesium oxides [11]. This slag layer provides a secondary benefit in that protects the molten iron from the heated air supplied via blast nozzles.

$$CaO + SiO_2 \rightarrow CaSiO_3 \tag{1}$$

Coke is coal that has undergone an energy-intensive heat treatment in an oxygen-deficient environment to raise the carbon concentration and remove volatile components such as benzene and ammonia [12]. The resulting carbon content can be 90 percent and greater. This carbon enrichment is needed, as it serves as the fuel for the chemical reduction process. Preheated air is supplied to the blast furnace near the bottom, as it is needed for the partial combustion reaction of the coke, and the concomitant production of the actual reducing species, such as carbon monoxide..

To yield 1 kg of crude iron from this process, approximately 2 kg of ore, 1 kg of coke, 0.3 kg of limestone, and 1.5 kg of air are required [9]. Depending on the quality of ore used, refining and heat treatment may be required to form pellets of acceptable hardness for use in the blast furnace. This is a prime example of a material- and energy-intensive industrial process.

The carbon in the coke and the oxygen supplied in the lower part of the blast furnace react to form carbon monoxide by Equation 2.

$$2C + O_2 \rightarrow 2CO \tag{2}$$

This reaction is exothermic with a -32.808 kcal/mol change in standard free energy, and provides the heat needed for furnace operation. The temperature can be controlled through the precise control of moisture in the supplied air, as it reacts endothermically in the manner shown in Equation 3.

$$C + H_2O \rightarrow CO + H_2 \tag{3}$$

The limestone charged into the top of the blast furnace decomposes into CO_2 and CaO. The iron ore is reduced by carbon monoxide by Equation 4 as well as by hydrogen as in Equation 5 among others.

$$Fe_3O_4 + 4CO \rightarrow 3Fe + 4CO_2 \tag{4}$$

$$Fe_3O_4 + 4H_2 \rightarrow 3Fe + 4H_2O \tag{5}$$
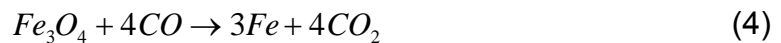
The generated heat and reduction of iron ore results in a distinct layer of molten iron at the bottom of the furnace covered by a layer of slag. The formation of molten metal clearly indicates the furnace reaches temperatures in excess of the melting temperature of iron, ~1540 C. Port locations are located to tap these layers individually, allowing the distinct removal of molten iron and waste products. The molten iron resulting from this process is typically used for the manufacture of steel through the use of alloying agents.

The blast furnace process described here is suboptimal for on demand manufacturing, as it is a continuous process that is ill suited for production of the small quantities required for batch manufacturing.

2. Atomization

The ductility of metal makes it very difficult to grind or otherwise mechanically seperate bulk metal into particles smaller than approximately 50 microns. In contrast, non-ductile, that is brittle materials such as metal oxides, can readily be ground to the range of a single micron in size. Thus, very small metal particles are traditionally made from the molten form.

Atomization of liquids can be accomplished hydraulically, where the liquid is forced through a nozzle by high pressure into a relatively stationary gas, or pneumatically, where a high velocity gas stream imparts the required energy to a stationary liquid. In either case, the environment and temperature of the atomized liquid droplets is tightly controlled to yield solidified powders with the desired characteristics [13]. The two methods of atomization have been a great subject of study, including the impact of temperature and pressure on the created droplets [14], but there are fundamental limitations to these techniques. There is an inverse relation between applied pressure and particle size; the higher the forcing pressure, the smaller the particles. The pressures applied are maximized in industrial atomization processes. Further increases in pressure would risk physical destruction of the device. Yet, this still only produces average particles with dimensions in the tens of microns. Moreover, an unfortunate property of

9

these resulting particles is their tendency to relax by recombining, resulting in larger particles after the initial processing has been completed. Thus, it is difficult to form particles less than 20 micron average size even with atomization.

C.   ALTERNATIVE SHAR APPROACH

The novelty of the proposed technique is that the metal oxide stock is already in powder form, and is reduced by gaseous radicals. The absence of physical contact between the oxide and the reducing agent has the benefit of negating any type of post treatment separation process. Metal oxide particles can be produced simply through physical processes such as grinding and filtering, and there is no recombination effect of the oxide particles, as they exist in a more thermodynamically favored state than their reduced counterparts.

III.   EXPERIMENTAL METHODS

A.   EXPERIMENTAL SETUP

The protocols designed in this section were designed to test the central hypothesis: gas species generated by the thermal and/or catalytically assisted decomposition of hydrocarbons in an inert atmosphere can reduce metal oxides to a metallic state. Thus, the experimental setup consisted of these components: i) a first vessel in which the selected hydrocarbons/catalysts could be decomposed in an inert atmosphere under selected temperature conditions, and ii) a second vessel to hold metal oxides, which was in contact with the first vessel only via the gas phase. The equipment setup required for the execution of experiments consisted of the two vessels described above, an oven for temperature control, a tubular quartz reactor to house the two vessels, and the apparatus required to maintain atmospheric control of the process as shown in Figure 2.

The reactor, fabricated of quartz to withstand the temperatures utilized, was of these dimensions: 25 mm outer diameter, 22 mm inner diameter, 0.6 m in length. The ends of the reactor were sealed to a gas flow system that permitted the system to be purged of air, and then maintained under a flowing inert gas. The exiting gas was routed to a standard fume hood for safety.

The tube furnace used for these experiments was a model TF55035A-1, which is manufactured by Lindberg/Blue M out of Ashville, North Carolina. This unit is rated at 800 kW and has a maximum continuous operating temperature of 1100 C.

Figure 2.   Experimental Apparatus

The structure of the two vessels is key to the experiment. In all cases, the hydrocarbon, and in most cases both hydrocarbon and catalyst, were placed in an alumina boat (first vessel) measuring 90 x 16 mm at the opening, with a height of 12 mm. The second vessel, shown in Figure 3, was fabricated from either Grafoil, a commercial high purity (>99 %) graphite sheet of thickness 0.4 mm, described in more detail in [15].
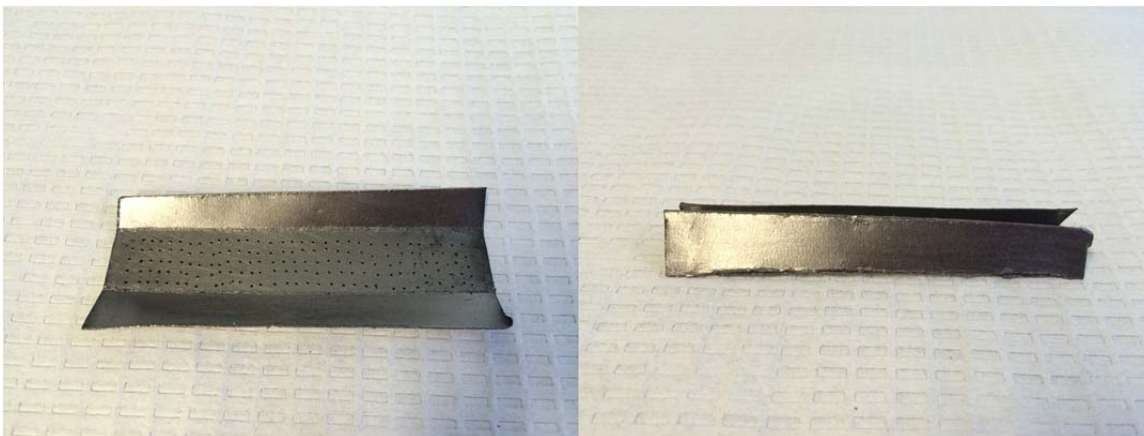
Figure 3.   Grafoil Sample Containment

Initially Grafoil was employed for the second vessel. A piece of Grafoil, of approximate dimensions 95 x 40 mm was fashioned to fit on top of the first vessel. The middle third was manually punctured with a sewing pin in an array of 5 rows of 32 holes measuring 0.6 mm in diameter to allow gas flow. The metal oxide powder was then contained in the folded Grafoil, and the loaded second vessel placed directly on top of the alumina boat / first vessel. When inserted into the quartz tube, the folded Grafoil placed the assembled sample under slight compression, aiding in stability when transitioning the tube to and from the oven.

Later experiments with iron oxide employed T304 stainless steel mesh, basically fashioned into the same shape as that shown for Grafoil, shown in Figure 4, and tightly fitted to the top of the alumina boat. Specifically, the 200 x 200 per 2.54 cm mesh is made from 0.0533 mm diameter wire, which has openings measuring 0.07 mm, for an opening area percentage of 33.6%. This item is stocked under the part number 200X200S0021W48T by TWP Inc. in Berkeley, California. The stainless steel mesh was folded in three segments similar to the Grafoil it replaced.
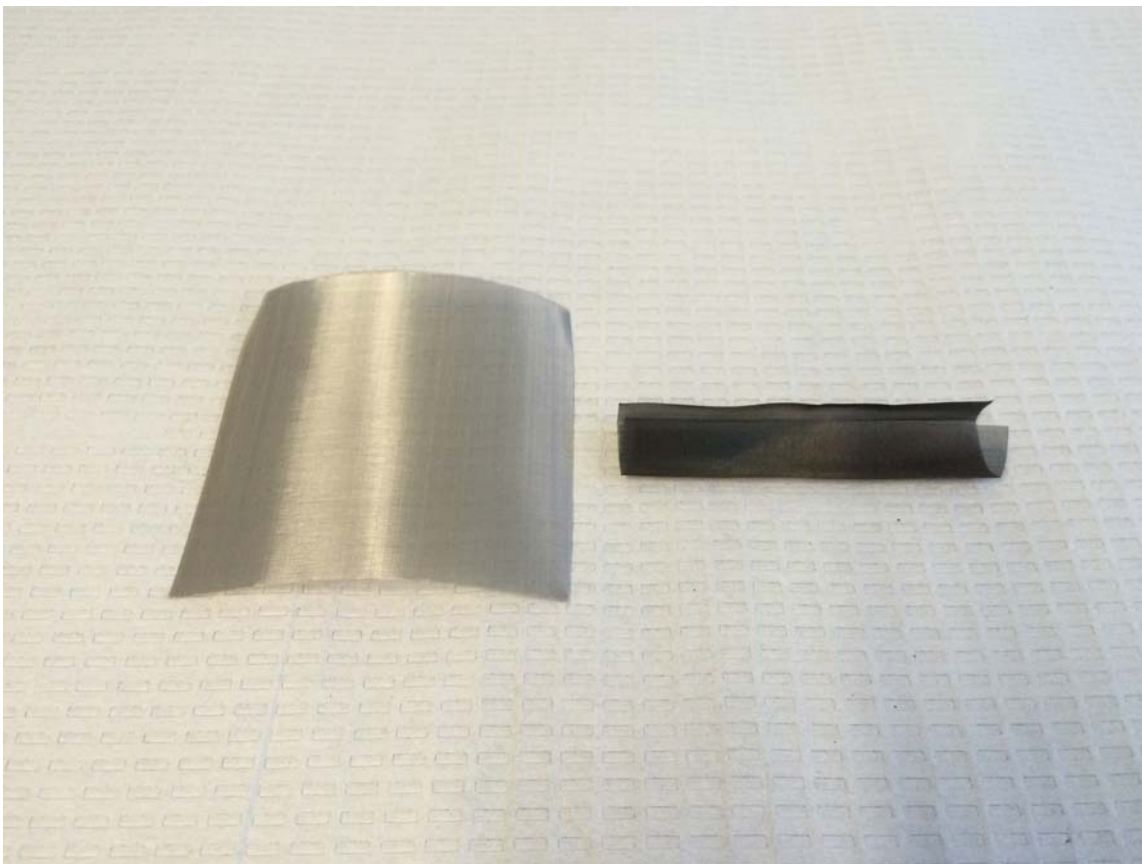
Figure 4.   Stainless Steel Mesh and Sample Containment

The reducing agent, composed of a hydrocarbon or a hydrocarbon / catalyst physical mixture, was prepared by first measuring the appropriate amount of hydrocarbon / catalyst to be used via a standard balance. The chosen hydrocarbon source and catalyst (if desired) was mixed thoroughly by stirring in an alumina boat. The second vessel was loaded with the desired amount of metal oxide powder. Generally, there was a simple mass relationship between the reducing agent and the metal oxide powder.

B.   EXPERIMENTAL PROCESS

The quartz tube was staged in front of the oven, and the sample inserted from the right (or upstream) end approximately 10 cm. Both tube ends were then capped using a four piece Ultra-Torr Swagelok fitting which formed a tight seal via a compressed O-ring, leaving a smaller fitting suitable for securing standard 5

mm plastic tubing. The upstream fitting was connected to a regulated supply of clean compressed nitrogen (N_2) gas by plastic tubing, and the downstream fitting was used to route plastic tubing to a standard laboratory fume hood.

The apparatus was then purged with N_2 gas for a nominal period of 20 minutes at a flow rate of 100 cc/min. The flow of N_2 gas was controlled using a FM-1050 series high accuracy flowmeter manufactured by Matheson Tri-Gas, part number ME14C201I200. At the completion of the purge period, the N_2 gas flow rate wa reduced to 10 cc/min, and flow was again verified. The flow rate of N_2 gas was maintained at 10 cc/min for the remainder of the experiment.

When the tube furnace reached the desired temperature of 850 C, the quartz tube was inserted such that the upstream end containing the sample remained external to the furnace. Once the furnace temperature stabilized, the sample heat cycle was commenced by simply sliding the tube to the left, ensuring the sample was near the center of the pre-heated furnace. Compact fans were staged to cool the Ultra-Torr Swagelok fittings during the heat cycle to protect the O-rings from thermal damage. The heat cycle was complete after 10 minutes, and the tube was removed with the aid of heat resistant gloves. The tube was then allowed to cool to room temperature, while maintaining the 10 cc/min N_2 flow.

Once the sample is cool, the Swageloks were disassembled, and the sample was removed. The treated metal oxide was then weighed and quickly placed in a glass vial. The vial was purged with clean Argon gas for a period of 10 to 15 seconds to displace the atmospheric gasses, capped tightly and sealed with Parafilm. This process of handling and storage was executed to minimize the exposure of the sample to the environment, which could result in re-oxidation of reduced metal powder created by the experiment.

The residual material that remains in the alumina boat was also weighed and retained in a separate vial. This residual material was stored by lightly capping the vial, with no Ar purge or sealing film used.

The first few experiments were used to test the effectiveness of the experimental apparatus as much as the result of the reaction. The only deficiency noted in this phase was the potential to clog the downstream plastic tubing with the products of the reaction. To mitigate this risk, the process was modified to include the cleaning of the downstream section of plastic tubing and cleaning all surfaces of the Ultra-Torr fitting prior to use. This method proved to be sufficient to prevent clogging.

1.   Variables and Controls

The experiment was conducted with many variable parameters that could be manipulated to optimize the results, but the combination of sample materials was the variable that receives the most scrutiny here. Three separate solid hydrocarbon sources were utilized: common candle wax, paraffin wax, and coal. The coal used in this case is low quality brown coal, or lignite. Two different catalysts were chosen for this experiment, sodium carbonate monohydrate ($Na_2CO_3 \cdot H_2O$) and potassium carbonate (K_2CO_3). Each solid hydrocarbon and catalyst combination was tested. Control experiments for each solid hydrocarbon with no catalyst were also performed. The set of experiments were performed using magnetite or iron oxide (Fe_3O_4) and nickel oxide (NiO) as targets for reduction. As the combination of materials shown in Table 1 chosen was the variable of focus, the mass of each constituent was held close to equal as possible. A target mass of 0.3 g for each ingredient was chosen, as the volume of the alumina boat used to contain the hydrocarbon and catalyst mixture was a limiting factor.

Table 1.   Investigated Material Species

Oxides	Hydrocarbons	Catalysts	Temperature (C)
NiO	Candle Wax	Na_2CO_3	850
Fe_3O_4	Paraffin	K_2CO_3	950
	Lignite	None	

The atmosphere control strategy of purging the quartz tube with N_2 gas at a rate of 100 cc/min for 20 minutes and maintaining a flow rate of 10 cc/min was utilized for all experiments. Changing the purge flow rate, duration, or the static flow rate for the execution of the heat cycle was not chosen as a variable of interest. Choosing a different purge gas, such as argon may be of interest in future experiments, as it is heavier than N_2 and is a more effective displacer of oxygen.

The heat cycle of 850 °C for 10 minutes was utilized for the initial set of experiments. This was chosen as the candle wax and paraffin wax would melt and provide the appropriate hydrocarbon and catalyst interaction for the experiment.

2.   Materials and Equipment

The materials utilized for this study include magnetite powder (Iron(II,III) Oxide powder, < 5 μm, 95%, CAS 1317-61-9) and nickel oxide powder (Nickel (II) Oxide green, -325 mesh, 99%, CAS 1313-99-1) as the source material, with sodium carbonate monohydrate (99.5%, A.C.S. reagent, CAS 5968-11-6) and potassium carbonate (99.995% trace metals basis, CAS 584-08-7) as catalysts. The solid hydrocarbon sources selected were wax from a dye free unscented candle, premium candle wax manufactured by Yayley Enterprises, and lignite coal sourced from the National Institute of Carbon in Oviedo, Spain.

The two forms of wax were sourced from a local arts and crafts store, and did not require any special storage or handling. The lignite was maintained in a sealed plastic bag that was evacuated using a hand pump. The bag was then secured inside a second evacuated bag, and stored in a commercial freezer for long-term storage.

All weight measurements were performed on an Ohaus Explorer Pro balance, model number EP114C, utilizing Schleicher & Schuell weighing paper (Z134120).

The Grafoil used to house the metal oxide during the experimentswere sourced from Fralock, which operates out of Valencia, California.

The interface between the quartz reactor and the gas flow apparatus is made up of a four-piece Ultra-Torr fitting from Swagelok and 5mm plastic tubing. The threaded male fitting and tubing were fastened together with a wrench, and then the remaining components slid onto the quartz reactor. With the male fitting held snugly against the reactor face, the female fitting is gently used to guide the O-ring into place, before being tightened hand-tight. The O-ring is compressed to create a strong seal. The flow of N_2 is verified by the formation of bubble at the submerged end of the apparatus, making a soap bubble type test at this union unnecessary.

When assembled, the fitting provides a convenient interface with easily replaceable plastic tubing. This proved to be valuable, as the downstream tubing can become clogged by deposits resulting from the experiments, and can become very stiff after many heat cycles from exhausted gases.

Assorted standard lab equipment such as spatulas and cleaning wipes were used as well, but do not warrant an itemized accounting.

3. Revisited Parameters

The initial set of experiments using formed Grafoil for the second vessel showed the nickel oxide could be completely reduced, but that magnetite powder was only partially reduced (see Results). This led to efforts to increase the reduction of the iron by using higher temperatures, a two step temperature process, a second vessel made of stainless steel screen, and relatively larger reducing mixtures.

In particular, additional experiments were conducted where the heat cycle was modified as follows. The sample preparation and handling was maintained from previous experiments, with catalytically promoted coal, but the temperature was initially set to 500 C. The sample was treated at this temperature for one

minute, and then removed from the furnace by sliding the tube. The oven was then set to maintain a temperature of 950 °C and allowed to stabilize. The sample was then reinserted into the oven and heated at this temperature for a period of five additional minutes, before being allowed to cool to room temperature prior to removal. This heat cycle was chosen serve dual purposes. First it was postulated that during the low temperature heat treatment the catalyst would spread on the coal surface. It was anticipated this would give rise to the second improvement: optimal catalytic efficiency and hence faster release of reducing species (e.g., CO) during the subsequent elevated temperature treatment.

The purpose of the change to stainless steel mesh for the second volume was both for effectiveness and consistency. The mesh has a more uniform array of holes through which the solid hydrocarbon and catalyst byproducts could pass through and interact with the metal oxide, while being small enough to prevent spillage into the alumina boat below.

In addition to the modified heat cycle, the amount of solid hydrocarbon and catalyst was increased for these experiments. While maintaining a target amount of 0.3 grams of metal oxide, the mass of lignite and catalyst used was doubled, and then tripled. This was performed exclusively on magnetite powder, as nickel oxide was successfully reduced with methods used in the initial set of experiments.

THIS PAGE INTENTIONALLY LEFT BLANK

IV. CHARACTERIZATION

Several characterization techniques were used to determine the effectiveness of the SHAR process, including scanning electron microscopy (SEM), energy dispersive x-ray spectroscopy (EDS) and x-ray diffraction (XRD).

A. SCANNING ELECTRON MICROSCOPY

The SEM utilized in this study is a Zeiss Neon 40 field emission SEM with focused ion beam. This microscope is equipped with backscattered electron (BSE) and energy dispersive analysis of x-rays (EDAX) detectors, and has a resolution of 1.1 nm using a 30 kV accelerating voltage.

All samples for this study were in loose powder form. Samples were installed on conductive sample mounts using double-sided carbon tape to allow for secure control of the sample position during analysis.

1. Method

Conventional optical light microscopy samples images via the light reflected from the object under inspection, and is inherently limited by the diffraction limit of photons in the visible spectrum. In contrast, SEM uses electrons that are not subject to this limitation to create the sample image. The limitation of optical microscopy is based on the wavelength of light in the visible spectrum, leading to a maximum magnification on the order of 2000x [16]. Beyond this region, increased magnification does not yield more information about the sample. Electrons with wavelength of 0.5 angstroms yield a theoretical limit of magnification of several hundred thousand, though practical limits are on the order of 75,000x. This practical range enables the imaging of materials on the nanometer scale. In addition to high resolution, the working distance used for sample analysis can be altered to obtain images with high depth of field, where the topography of the sample can be simultaneously in focus [17].

Materials to be imaged via SEM are placed under high levels of vacuum: 1E-5 Torr for the chamber, and 3E-10 Torr for the gun. This effort reduces the gas molecules in the chamber, which otherwise would scatter the generated electron beam. Other types of gaseous contaminants could deposit on the specimen under investigation if the chamber is not effectively evacuated [18].

The generated electrons are accelerated by a voltage source on the range of 1 to 30 keV in most SEMs [16], determined by the material being inspected. 20 keV was used for the images that follow. The resulting electron beam is variable up to approximately 200 Å in diameter, while smaller diameter electron beams are critical for high-resolution image capture.

The generation of the SEM image is generated similarly to the line-by-line drawing of an image on a cathode ray tube (CRT) display. The user can adjust the scan speed of the electron beam, or the rate at which the beam passes over the sample. The quality of the image is inversely proportional to the scan speed. In practice, a fast scan speed is used to generate a displayed image adequate for identifying areas of interest. Once an area is selected for detailed investigation, the scan speed is reduced for high quality image capture.

2. Analysis

The SEM was used to capture images of both the untreated iron and nickel oxides as well as treated samples of interest. This allowed direct comparison size and morphology of the powders resulting from the experiment to their untreated state.

a. Imaging

Images were captured for each sample at a resolution of 2048x1536 using a scan speed of 4 and line integrated noise reduction. To ensure a level of consistency and comparability, each sample analyzed was captured at 12,500x at multiple locations, as well as at 5,000x. The high magnification images were

captured to show morphology and geometry of the powders, whereas lower magnification images were used for larger scale comparison.

b. Energy Dispersive X-Ray Spectroscopy

The EDAX detector equipped on the SEM allows for a compositional analysis of the sample. When the electron beam interacts with the sample, the incident atoms can become excited, elevating electrons to a higher energy state. The electron will naturally de-excite to regain its more stable ground state through the emission of a photon. The energy of this photon is precisely the same as the difference in the electron energy states, which are in turn characteristic of the element.

Through the collection of these emitted de-excitation photons, a spectrum can be constructed, and the relative intensity of the peaks can be related to the relative quantity of the present elements.

The area scanned for EDS analysis is set by the same method as for SEM image capture. In each case, a zoom of 500x was selected to get a representative result of the sample, instead of only a few select particles at high magnification.

Although useful, it is important to note that this analysis provides a literally superficial result, due to the low penetration of the incident radiation. Additionally, the resulting atomic fraction provides no information about the phase or crystal structure of the sample under investigation. This analysis was used primarily to support and validate the results found via XRD.

B. X-RAY DIFFRACTION (XRD)

The X-ray diffraction characterization technique was critical to evaluating the success of the experiments, as it yields the relative composition of the processed sample. Unlike EDS methods that result in relative abundance of elements, XRD is used to identify the crystal structures present in the sample. For example, EDS may show percentage of elemental iron and oxygen present,

23

where XRD will explicitly determine the components and phase in which they appear – Fe_3O_4, Fe_2O_3, FeO, Fe and so on.

1. Method

The principle of XRD characterization is the identification of constructively scattered x-rays. A precisely known x-ray source is made incident upon the sample, resulting in scattering reactions at various angles. If the target has a consistent crystal structure, there is a condition that promotes constructive interference in the scattered x-ray.

The yield from the experiments was low due to physical limitations of the reactor and enclosed containment, so it was necessary to use a special zero background holder with a small depression in the center, shown in Figure 5.

Figure 5.   Zero Background XRD Sample Holder

A portion of the processed oxide powder was placed in the depression and compressed using a clean glass microscope slide. The depression was filled with compressed powder and the excess carefully removed. The samples were scanned directly after preparation to minimize the potential of reoxidation of

reduced metal. Additionally, the characteristic spectra associated with the anticipated forms of oxide and reduced metal were compared to determine a range of angles to scan the sample that would provide sufficient peaks while ensuring the peaks were distinguishable. The processed magnetite samples were scanned over the range of angles from 10 to 90 degrees, while the processed nickel oxide samples were scanned from 25 to 100 degrees. In all cases, the angle rate was chosen to be 10 degrees per minute, resulting in scans of less than 10 minutes per sample. The spectra from these parameters were sufficiently useful for phase identification while minimizing the exposure of the sample to the atmosphere over the duration of the scan.

The Rigaku Miniflex 600 X-Ray Diffractometer source uses the Cu K_α x-ray, which has characteristics of 8.04 keV and a wavelength of 0.1542 nm [19]. For each analysis, the instrument was operated at a voltage and current of 40 kV and 15 mA, respectively.

2. Analysis

Figure 6 shows a lattice structure with interplanar spacing d_{hkl}. For the scattered x-rays to be in phase, the distance traveled must differ by an integer factor of the wavelength.
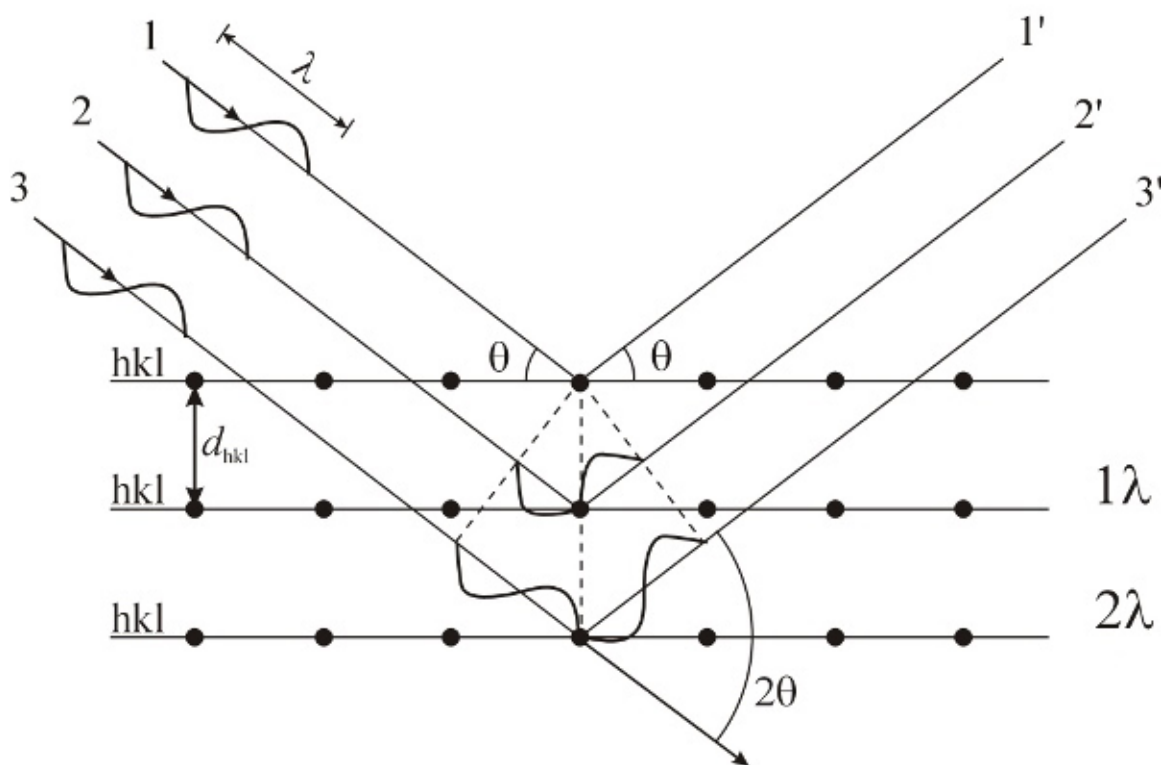
Figure 6.   Bragg Scattering Geometry, after [19]

Simple geometric analysis of this condition yields the familiar Bragg law in Equation 6.

$$n\lambda = 2d_{hkl}\sin(\theta) \tag{6}$$

The wavelength of the incident x-ray source is known, making this interference condition purely a function of crystal plane spacing. The identities of the phases present in the sample are then determined by comparing the spectrum peaks with documented values available in various publications. For this study, the spectra was compared against a database using PDXL software.

When the sample is subjected to the x-ray source, it is possible for the x-ray to be absorbed by an orbital electron, raising the atom to an excited state. The excited atom can return to its ground state by emitting a photon of energy equal to that of the incident beam. In this case, the emitted photon is called fluorescent radiation [19]. This radiation is not direction specific, so it has the

effect of obscuring the otherwise distinct peaks predicted by bragg scattering, as shown in Figure 7.
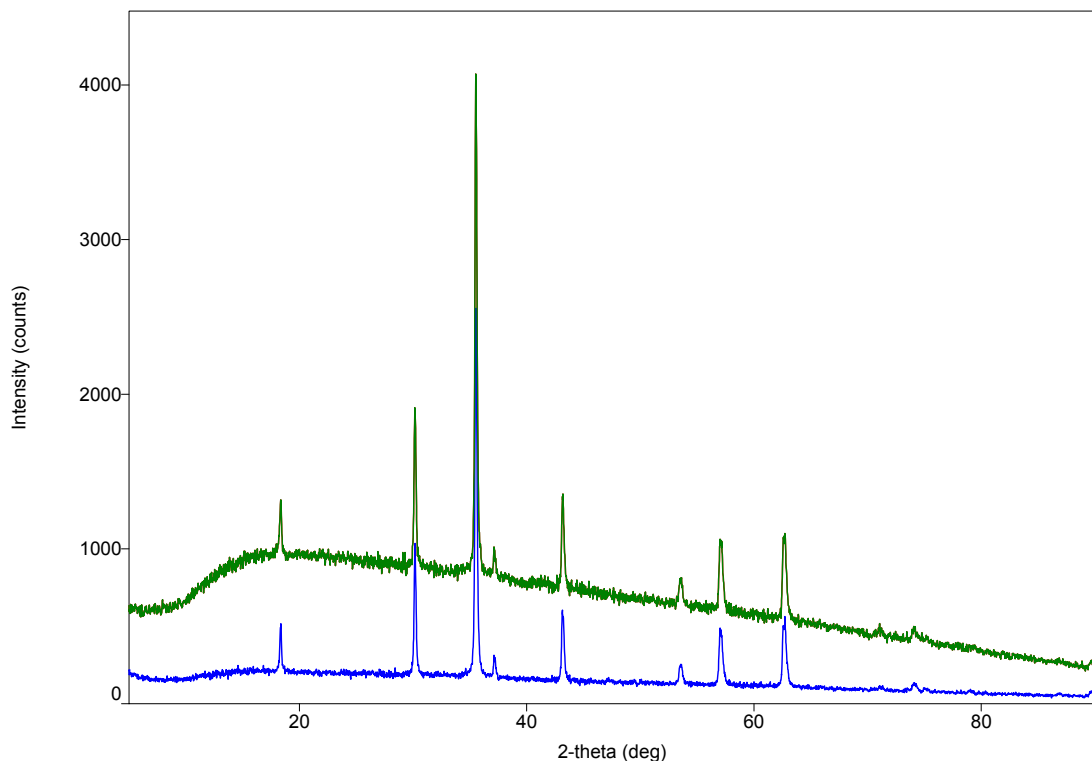
Figure 7.   Magnetite XRD Spectrum (Green), Fluorescence Corrected (Blue)

In this case, untreated magnetite has been characterized by XRD, yielding the plot in green, which is subject to fluorescent radiation. This radiation can in some cases make it impossible to resolve the peaks characteristic of the sample due to low intensity. The fluorescence effect has been reduced for the plot of the same scan, this time in blue. This is accomplished by altering the pulse height analyzer to a smaller window. Although the peaks are slightly smaller, the effect of reducing the fluorescence is to greatly improve the peak to background ratio.

Finally, the impact of background radiation that is detected during the scan is compensated for, resulting in the ultimate result shown in Figure 8.
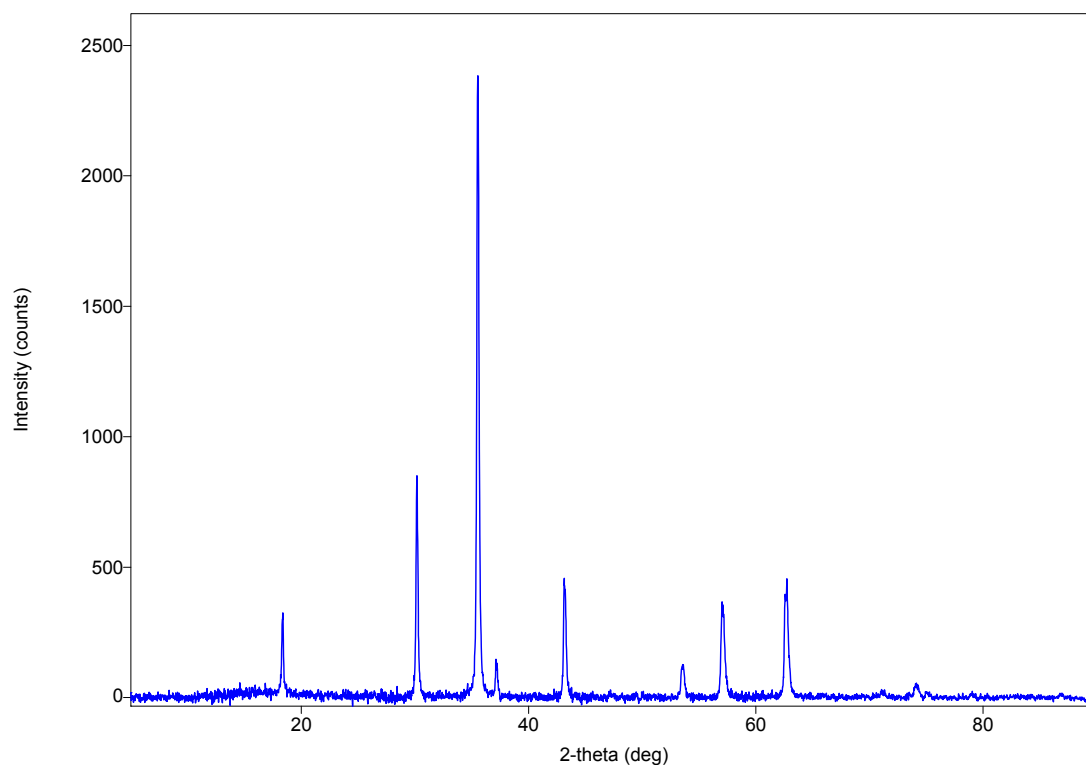
Figure 8.   Magnetite XRD Spectrum–Fluorescence and Background Corrected

The end result of these improvements is to improve the ability of the software to identify small intensity characteristic peaks that may otherwise be indistinguishable. Each sample analyzed for this study was treated in this fashion.

V.   RESULTS

XRD characterization was conducted to determine the efficacy of the SHAR technique, the results of which are included. SEM images for characteristic samples are included as well to give insight into the structure and size of the resulting particles.

A.   XRD ANALYSIS

X-ray diffraction is the primary characterization method used to determine the metal phases present before and after SHAR treatment. The XRD data provides quantification of the extent of reduction, which is the objective of the SHAR process. Thus it is a measure of the effectiveness of reducing metal oxide powders using the SHAR technique. The results of these analyses are included for review, beginning with the untreated metal oxides.

1.   Untreated Metal Oxide

The source iron and nickel oxides were subjected to 850 °C for 10 minutes with no hydrocarbon or catalyst in the reactor. No reduction was expected, and none was observed by X-Ray Diffraction analysis.

The XRD spectrum for the control experiment for nickel oxide is shown in Figure 9, with spectrum details in Table 2.
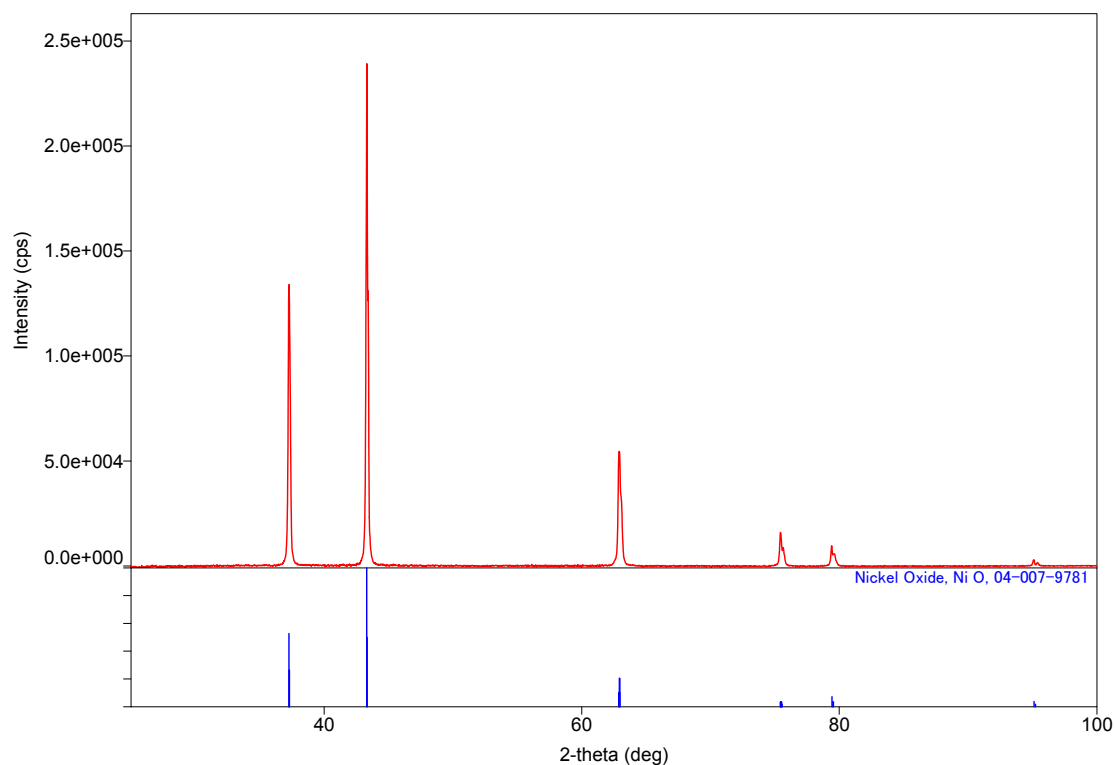
Figure 9.   Nickel Oxide XRD Spectrum–Control Experiment

Table 2.   Nickel Oxide (NiO) Spectrum Data–PDF card 04-007-9781

No.	2-theta(deg)	d(ang.)	Phase name
1	37.2720(13)	2.41053(8)	Nickel Oxide(1,1,0)
2	43.3182(11)	2.08705(5)	Nickel Oxide(1,1,-1)
3	62.9115(17)	1.47612(4)	Nickel Oxide(0,2,0)
4	75.4389(19)	1.25907(3)	Nickel Oxide(0,2,1)
5	79.389(4)	1.20605(6)	Nickel Oxide(2,2,0)
6	95.099(5)	1.04396(4)	Nickel Oxide(2,2,-2)

The XRD spectrum for the control experiment for iron oxide is shown in Figure 10, with spectrum details in Table 3. Note that all peaks are accounted for, and that the relative intensities observed are those expected from a powder with no preferential orientation.
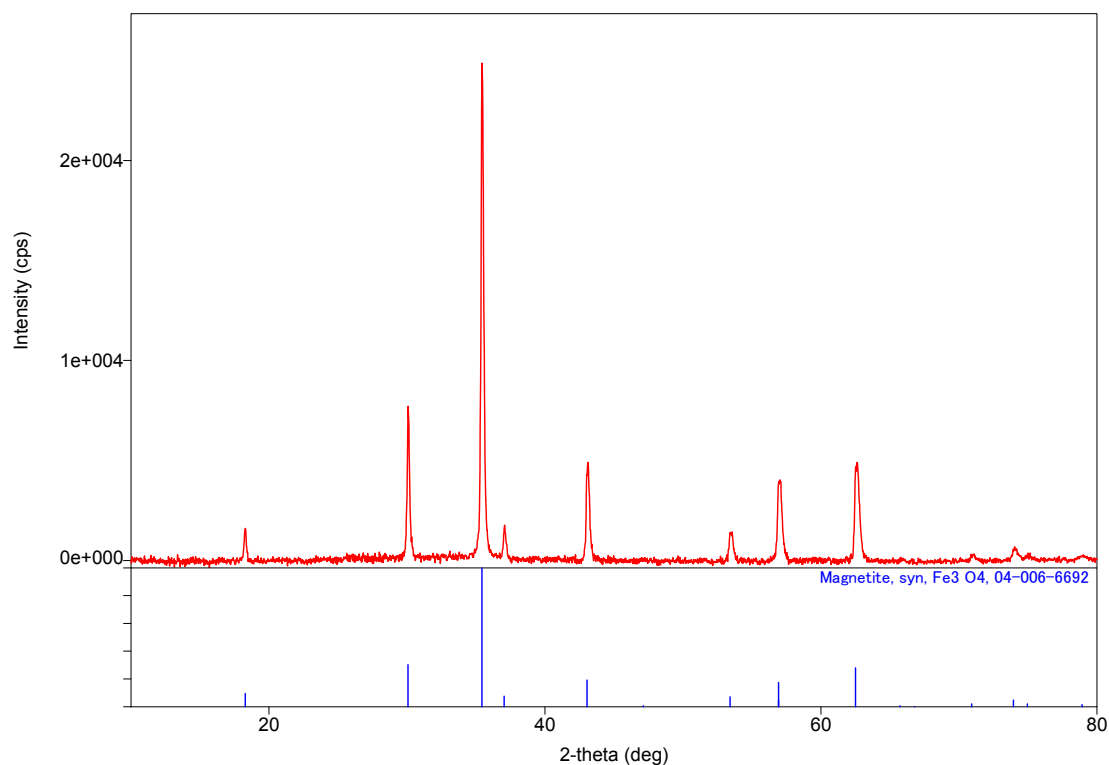
Figure 10. Magnetite XRD Spectrum–Control Experiment

Table 3.   Magnetite (Fe_3O_4) Spectrum Data–PDF card 04-006-6692

No.	2-theta(deg)	d(ang.)	Phase name
1	18.269(12)	4.852(3)	Magnetite, syn(1,1,1)
2	30.091(5)	2.9674(5)	Magnetite, syn(2,2,0)
3	35.430(3)	2.53155(18)	Magnetite, syn(3,1,1)
4	37.060(7)	2.4238(5)	Magnetite, syn(2,2,2)
5	43.033(6)	2.1002(3)	Magnetite, syn(4,0,0)
6	53.45(2)	1.7128(7)	Magnetite, syn(4,2,2)
7	56.925(7)	1.61628(19)	Magnetite, syn(3,3,3)
8	62.509(6)	1.48465(12)	Magnetite, syn(4,4,0)
9	73.93(3)	1.2811(5)	Magnetite, syn(5,3,3)

2.   Hydrocarbon Control Experiments: No Catalyst

Evaluation of catalyst performance requires control experiments using hydrocarbon and no catalyst. Paraffin was chosen as the hydrocarbon for these experiments.

These experiments resulted in partial reduction of the magnetite powder, and complete reduction of nickel oxide powder as shown in Table 4, suggesting the thermal decomposition of paraffin alone was sufficient for reduction.

Table 4.   XRD Results: Catalyst-free Control Experiments

Reactants			Products			
Oxide	Hydrocarbon	Catalyst	NiO (%)	Ni (%)	Fe_3O_4 (%)	FeO (%)
NiO	pWax	N/A		100.0(4)		
Fe_3O_4	pWax	N/A			86.6(4)	13.4(3)

The XRD spectrum for the catalyst-free paraffin experiment for nickel oxide is shown in Figure 11, with spectrum details in Table 5.
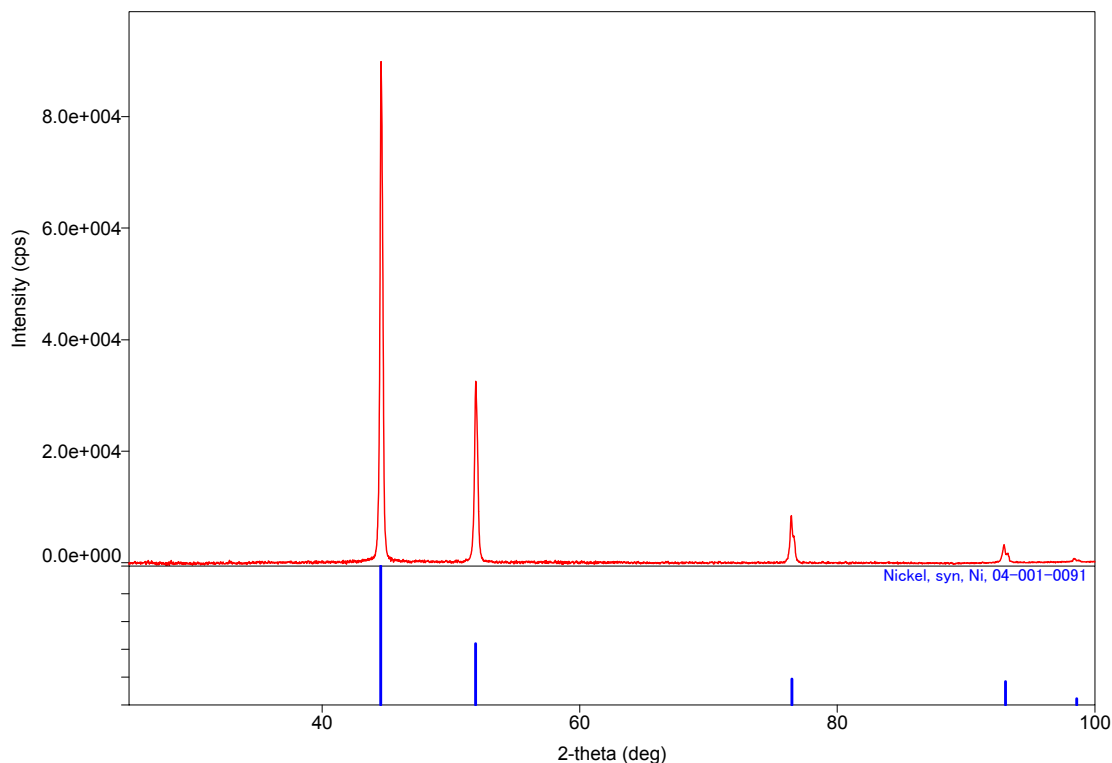
Figure 11.   Fully Reduced Nickel XRD Spectrum

Table 5.   Fully Reduced Nickel Spectrum Data–PDF card 004-001-0091

No.	2-theta(deg)	d(ang.)	Phase name
1	44.5842	2.03068	Nickel, syn(1,1,1)
2	51.93	1.75938	Nickel, syn(2,0,0)
3	76.4261	1.24525	Nickel, syn(2,2,0)
4	92.9565	1.06231	Nickel, syn(3,1,1)
5	98.3859	1.01768	Nickel, syn(2,2,2)

The XRD spectrum for the catalyst-free paraffin experiment for iron oxide is shown in Figure 12, with spectrum details in Table 6. In this case, the peaks characteristic of unreduced magnetite are marked in blue on the top row, while peaks associated with the partially reduced wustite (FeO) are marked in red in the bottom row. Once again the relative intensities observed are those anticipated from a powder in which there is no preferential orientation.
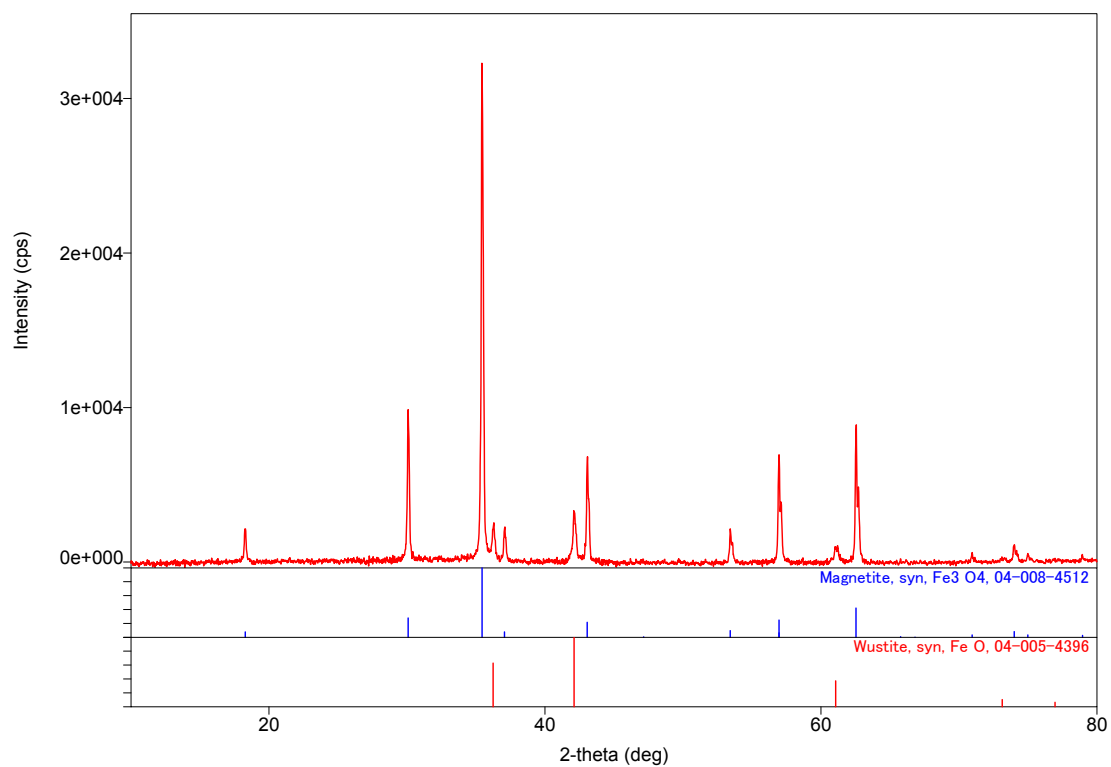
Figure 12. Partially Reduced Iron Oxide XRD Spectrum

Table 6.   Partially Reduced Magnetite Spectrum Data

No.	2-theta(deg)	d(ang.)	Phase name	Chemical formula	DB card number
1	18.2719	4.85143	Magnetite, syn(1,1,1)	Fe3 O4	04-008-4512
2	30.0898	2.96752	Magnetite, syn(2,2,0)	Fe3 O4	04-008-4512
3	35.4467	2.53036	Magnetite, syn(3,1,1)	Fe3 O4	04-008-4512
4	36.2931	2.47327	Wustite, syn(1,1,1)	Fe O	04-005-4396
5	37.0821	2.42244	Magnetite, syn(2,2,2)	Fe3 O4	04-008-4512
6	42.1103	2.14408	Wustite, syn(2,0,0)	Fe O	04-005-4396
7	43.0771	2.09818	Magnetite, syn(4,0,0)	Fe3 O4	04-008-4512
8	53.4565	1.71269	Magnetite, syn(4,2,2)	Fe3 O4	04-008-4512
9	56.9719	1.61507	Magnetite, syn(5,1,1)	Fe3 O4	04-008-4512
10	61.0336	1.51695	Wustite, syn(2,2,0)	Fe O	04-005-4396
11	62.5543	1.48368	Magnetite, syn(4,4,0)	Fe3 O4	04-008-4512
12	70.955	1.32722	Magnetite, syn(6,2,0)	Fe3 O4	04-008-4512
13	73.9776	1.28029	Magnetite, syn(5,3,3)	Fe3 O4	04-008-4512
14	74.9961	1.26541	Magnetite, syn(6,2,2)	Fe3 O4	04-008-4512
15	78.9173	1.21207	Magnetite, syn(4,4,4)	Fe3 O4	04-008-4512

Each treated metal oxide sample was analyzed using identical methods as the control experiments covered in detail above. The relative intensity of the peaks in the resulting XRD spectrum are used by the software to determine the percentage of the identified phases in each sample. The results of this relative intensity method are tabulated for further experiments, as the spectra are similar in nature to those already shown and provide little additional information.

3. Hydrocarbon and Catalyst Experiments

The experiments were then repeated using each combination of metal oxide, hydrocarbon and catalyst to allow for trend analysis. The physical data from these experiments are shown in Table 7. Included in this table is the reduction in mass of the combined hydrocarbon and catalyst mixture, calculated by the change in mass of the mixture divided by the original mass.

Table 7.   Physical data: Hydrocarbon and Catalyst Experiments

	Input					Output		
Oxide	Mass (g)	Hydrocarbon	Mass (g)	Catalyst	Mass (g)	Product Metal (g)	Residual Material (g)	Hydrocarbon and Catalyst Mixture Mass Reduction (%)
NiO	0.2998	Wax	0.3002	Na_2CO_3	0.2997	0.2590	0.2465	58.91
	0.2997	pWax	0.3003	Na_2CO_3	0.3001	0.2480	0.2512	58.16
	0.2997	Wax	0.3000	K_2CO_3	0.3002	0.2757	0.2902	51.65
	0.3000	pWax	0.2997	K_2CO_3	0.3002	0.2553	0.2912	51.46
Fe_3O_4	0.2992	Wax	0.3006	Na_2CO_3	0.2993	NDR	NDR	NDR
	0.3002	pWax	0.3002	Na_2CO_3	0.3005	0.2884	0.2471	58.86
	0.3003	Wax	0.3003	K_2CO_3	0.3004	0.281	0.2831	52.87
	0.3003	pWax	0.3003	K_2CO_3	0.3005	0.2799	0.2807	53.28

Table 8 collects the X-Ray diffraction analysis results for these experiments. Nickel oxide is shown to be generally more effectively reduced when compared to magnetite.

Table 8.   XRD Results: Hydrocarbon and Catalyst Experiments

Reactants			Products			
Oxide	Hydrocarbon	Catalyst	NiO (%)	Ni (%)	Fe_3O_4 (%)	FeO (%)
NiO	Wax	Na_2CO_3	100.0(3)			
	pWax	Na_2CO_3	3.2(4)	96.8(3)		
	Wax	K_2CO_3		100.0(2)		
	pWax	K_2CO_3		100.0(3)		
Fe_3O_4	Wax	Na_2CO_3			89.0(7)	11.0(3)
	pWax	Na_2CO_3			92.1(4)	7.9(3)
	Wax	K_2CO_3			48.1(5)	51.9(5)
	pWax	K_2CO_3			71.0(4)	29.0(4)

4.   Coal Control Experiments: No Catalyst

The experiments were repeated using the same methods, with low cost lignite as a hydrocarbon source. As with the paraffin control experiments, the thermal decomposition of coal was more effective at reducing nickel oxide than iron oxide. It must be noted, however, that catalytically promoted coal never fully reduced either the NiO or the Fe_3O_4, whereas using SHAR with paraffin wax, even without catalyst led to complete reduction of the NiO. The physical data and results of these control experiments are collected in Tables 9 and 10, respectively.

Table 9.   Physical Data: Catalyst-free Coal Experiments

	Input					Output		
Oxide	Mass (g)	Hydrocarbon	Mass (g)	Catalyst	Mass (g)	Product Metal (g)	Residual Material (g)	Hydrocarbon and Catalyst Mixture Mass Reduction (%)
NiO	0.2999	Coal	0.2997	N/A	0	0.2679	0.1820	39.27
Fe_3O_4	0.3003	Coal	0.3002	N/A	0	0.2885	0.1754	41.57

Table 10.   XRD Results: Catalyst-free Coal Experiments

Reactants			Products			
Oxide	Hydrocarbon	Catalyst	NiO (%)	Ni (%)	Fe_3O_4 (%)	FeO (%)
NiO	Coal	N/A	74.9(5)	25.09(13)		
Fe_3O_4	Coal	N/A			100.00(4)	

5.   Coal and Catalyst Experiments

Each combination of metal oxide powder and catalyst was tested using coal as the hydrocarbon source. The physical data for these experiments is contained in Table 11.

Table 11.   Physical Data: Coal and Catalyst Experiments

	Input					Output		
Oxide	Mass (g)	Hydrocarbon	Mass (g)	Catalyst	Mass (g)	Product Metal (g)	Residual Material (g)	Hydrocarbon and Catalyst Mixture Mass Reduction (%)
NiO	0.3003	Coal	0.3000	Na_2CO_3	0.2998	0.2444	0.4075	32.06
	0.3003	Coal	0.2997	K_2CO_3	0.3003	0.2733	0.4747	20.88
Fe_3O_4	0.3001	Coal	0.3003	Na_2CO_3	0.2997	0.2828	0.4194	30.1
	0.3003	Coal	0.2997	K_2CO_3	0.3002	0.2864	0.4707	21.54

Table 12 collects the X-Ray diffraction analysis results for these experiments.

Table 12.　XRD Results: Coal and Catalyst Experiments

Reactants			Products			
Oxide	Hydrocarbon	Catalyst	NiO (%)	Ni (%)	Fe_3O_4 (%)	FeO (%)
NiO	Coal	Na_2CO_3	23.8(3)	76.2(4)		
	Coal	K_2CO_3	82.6(4)	17.44(8)		
Fe_3O_4	Coal	Na_2CO_3			58.0(5)	42.0(4)
	Coal	K_2CO_3			100.00(4)	

The experimental results revealed that the process was consistently less effective at reducing iron oxide than nickel oxide under the same laboratory conditions.

6.　Modified Coal and Catalyst Experiments

The remainder of the experimental phase focused on improving the reduction of iron oxide powder. The heat treatment was modified to use a higher temperature of 950 °C and the grafoil containment was replaced with stainless steel mesh. The amount of coal and catalyst was doubled, and then tripled from previous experiments. The physical data for these experiments is compiled in Table 13.

Table 13.   Physical Data: Modified Coal and Catalyst Experiments

	Input					Output		
Oxide	Mass (g)	Hydrocarbon	Mass (g)	Catalyst	Mass (g)	Product Metal (g)	Residual Material (g)	Hydrocarbon and Catalyst Mixture Mass Reduction (%)
Fe$_3$O$_4$	0.3003	Coal	0.6003	Na$_2$CO$_3$	0.6003	0.2867	0.8537	28.89
	0.2998	Coal	0.6002	K$_2$CO$_3$	0.6003	0.2623	0.8935	25.57
	0.3003	Coal	0.8997	Na$_2$CO$_3$	0.8999	0.2872	1.3013	27.69
	0.2999	Coal	0.8998	K$_2$CO$_3$	0.9003	0.278	1.3615	24.37

Tables 14 and 15 contain the X-Ray diffraction analysis results for these experiments.

Table 14.   XRD Results: Coal and Catalyst Doubled

Reactants		Products			
Hydrocarbon	Catalyst	Fe_3O_4 (%)	FeO (%)	FeO (%)	Fe (%)
Coal	Na_2CO_3	37.2(4)	62.8(6)		
Coal	K_2CO_3		56(3)	37(3)	7.81(12)

It is notable that experiment using coal catalytically promoted by K_2CO_3 resulted in two distinctly identifiable forms of FeO with slightly differing interphase dimensions. The two forms of wustite identified for this experiment are characterized by PDF Cards 04-006-5424 and 04-003-5839.

Table 15.   XRD Results: Coal and Catalyst Tripled

Reactants		Products			
Hydrocarbon	Catalyst	Fe_3O_4 (%)	Fe_2O_3 (%)	FeO (%)	Fe (%)
Coal	Na_2CO_3	80.8(3)	19.2(3)		
Coal	K_2CO_3		34.9(11)	58(5)	7.37(12)

The results of this experimental phase illustrates that dramatically increasing the coal and catalyst content in the reactor volume was ineffective at improving the reduction of iron oxide powder.

B.   SEM ANALYSIS

Scanning electron microscopy was performed to identify structure and size of the powders created by the SHAR process. As with the XRD technique, the untreated metal oxides were analyzed for comparison. For each case, images were captured at 5000, 12,500, and 50,000 times magnification to provide consistency between samples.

## 1.	Untreated Nickel Oxide

Figures 13-15 show the structure and orientation of the untreated nickel oxide powder.
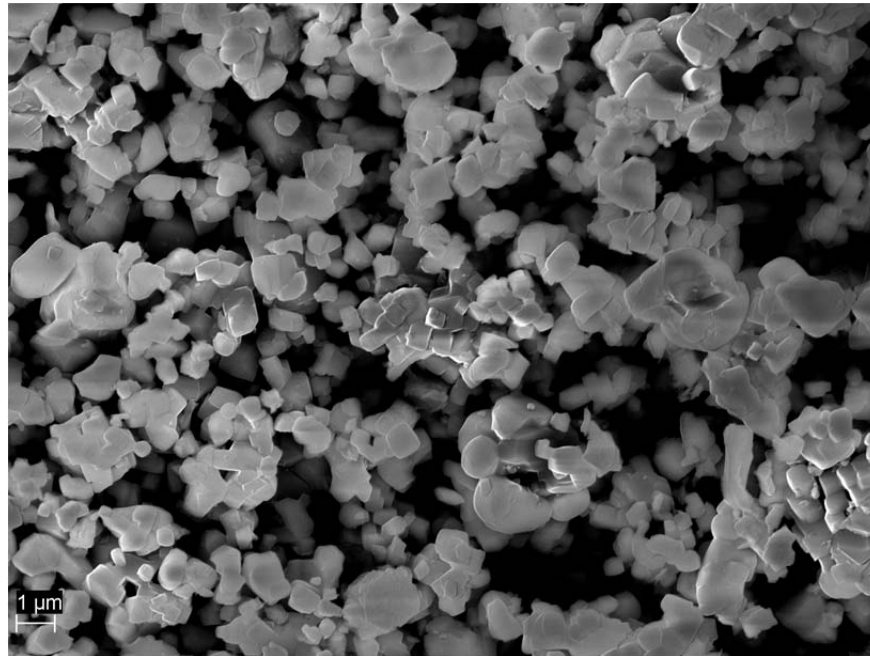

Figure 13.   Untreated Nickel Oxide 5k Magnification
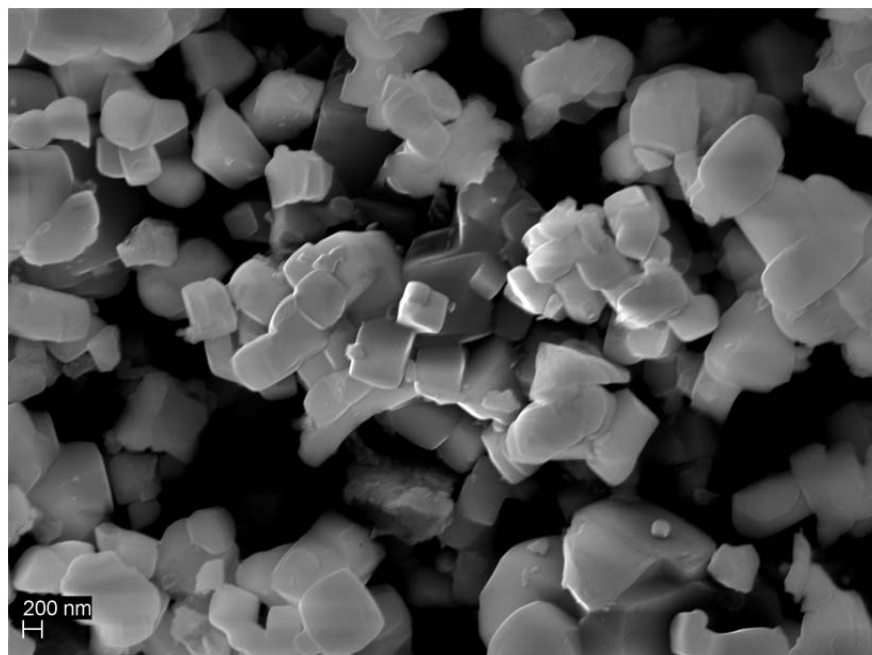
Figure 14.   Untreated Nickel Oxide 12.5k Magnification
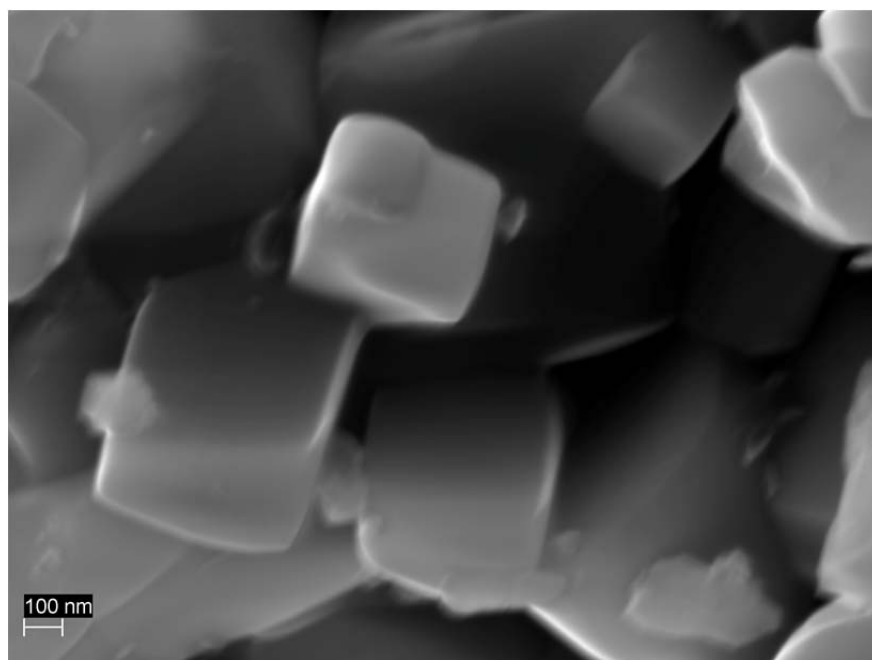
Figure 15.   Untreated Nickel Oxide 50k Magnification

These images show a high degree of symmetry, which is expected for the NiO crystal structure. Typical particle sizes for this untreated powder are on the order of 200-400 nm wide.

2. Fully Reduced Nickel

Figures 16-18 are images obtained for the nickel oxide sample processed with paraffin promoted with K_2CO_3, which experienced complete reduction.
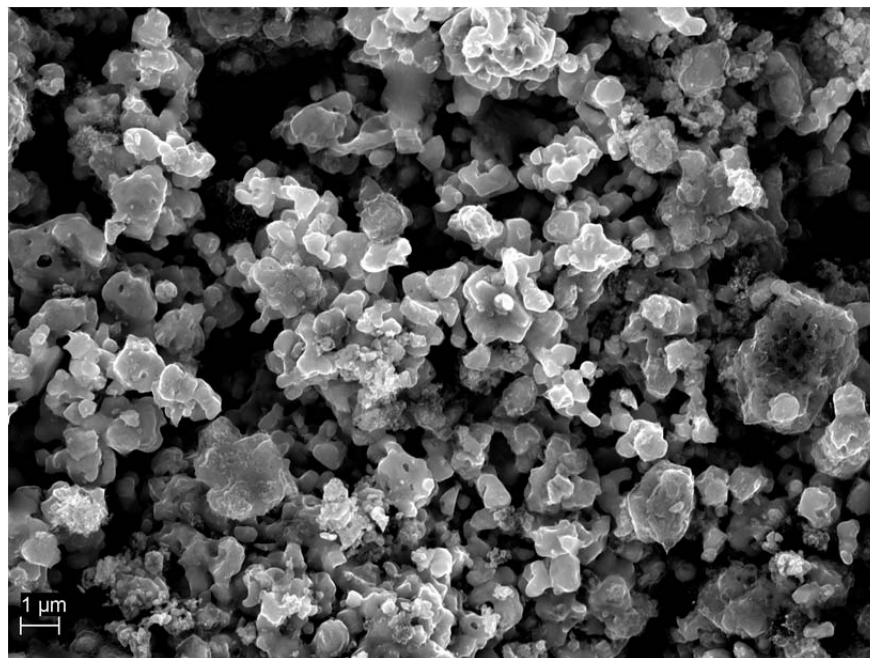
Figure 16.   Nickel Fully Reduced by Paraffin and K_2CO_3 5k Magnification
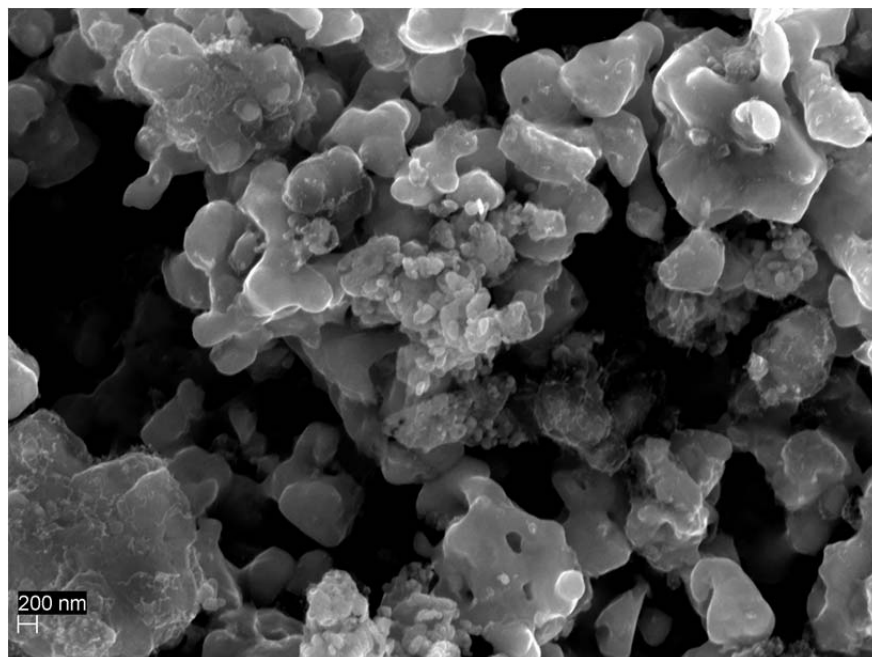
Figure 17.   Nickel Fully Reduced by Paraffin and K_2CO_3 12.5k Magnification
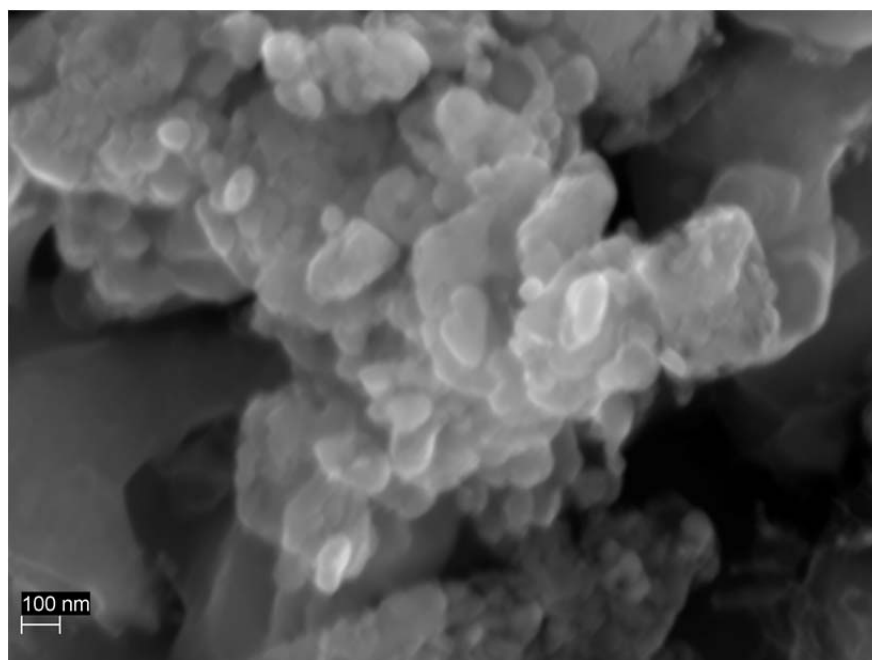
Figure 18.   Nickel Fully Reduced by Paraffin and K_2CO_3 50k Magnification

The fully reduced nickel powder exhibited a change in surface morphology, as the symmetry of the untreated oxide is no longer apparent. The

size of reduced particles remains on the same order of magnitude as in their untreated state.

3.   Untreated Magnetite

Figures 19-21 show the structure and orientation of the untreated magnetite powder.
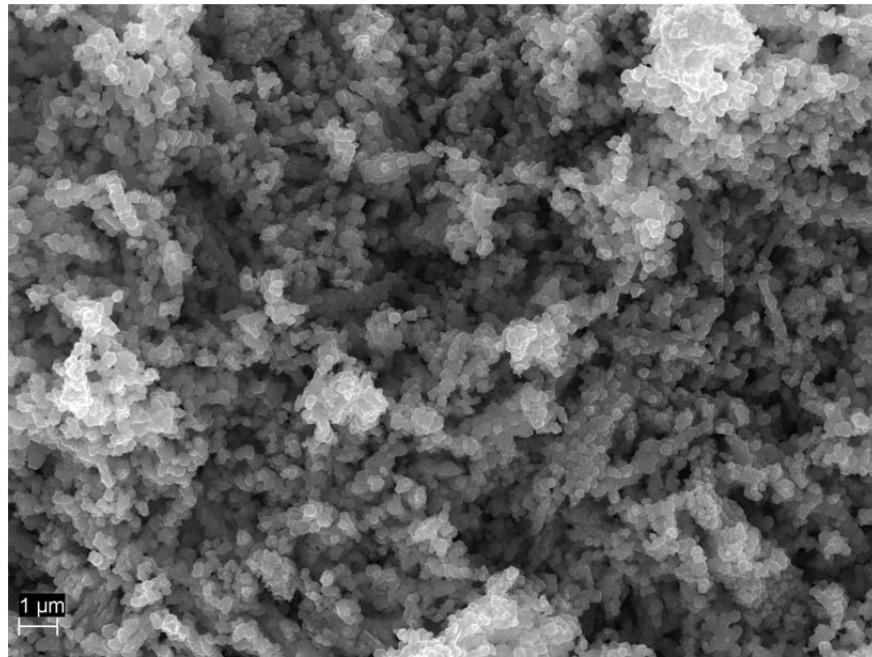

Figure 19.   Untreated Magnetite 5k Magnification
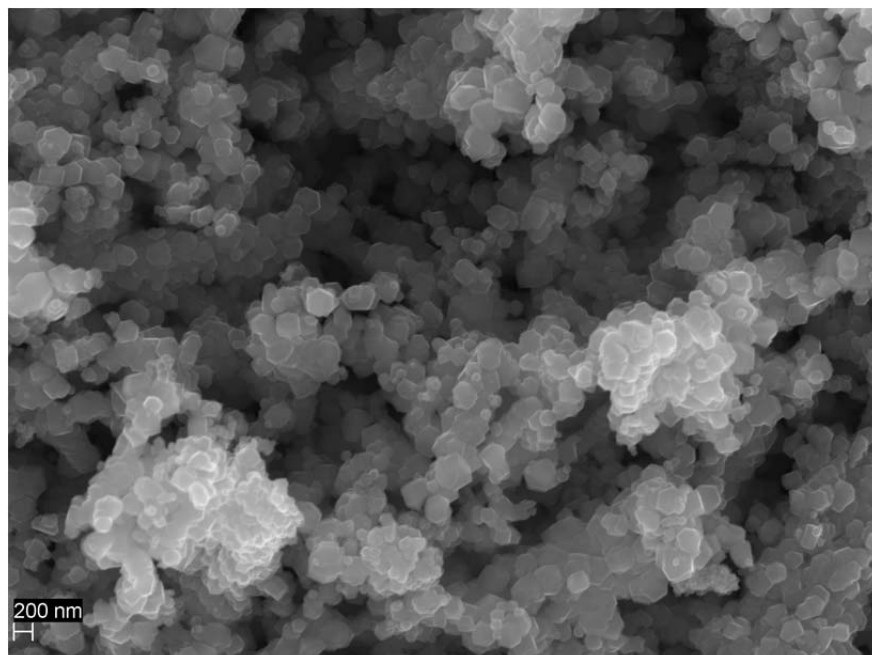
Figure 20.   Untreated Magnetite 12.5k Magnification
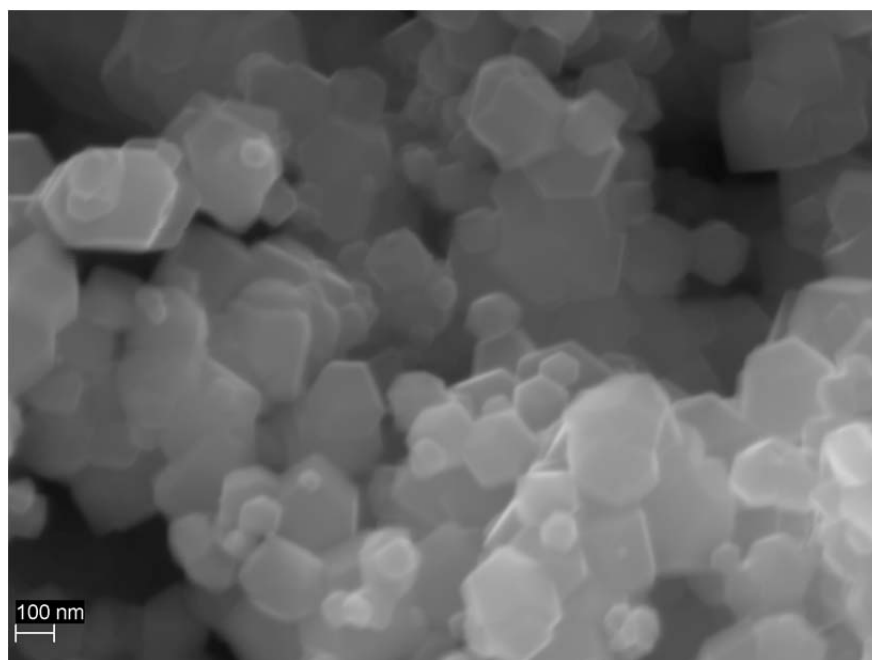
Figure 21.   Untreated Magnetite 50k Magnification

The untreated magnetite shows well-defined particle boundaries of highly regular shape, with sizes in the range of 100-300 nm.

4. Partially Reduced Magnetite

Although no experiment resulted in complete reduction of magnetite to iron metal, partial reduction was achieved. Figures 22-24 included here are a result of the experiment using a doubled amount of coal promoted by K_2CO_3, which resulted in reduction of the sample to two forms of FeO and a small amount (7.8%) of iron metal as shown in Table 14.
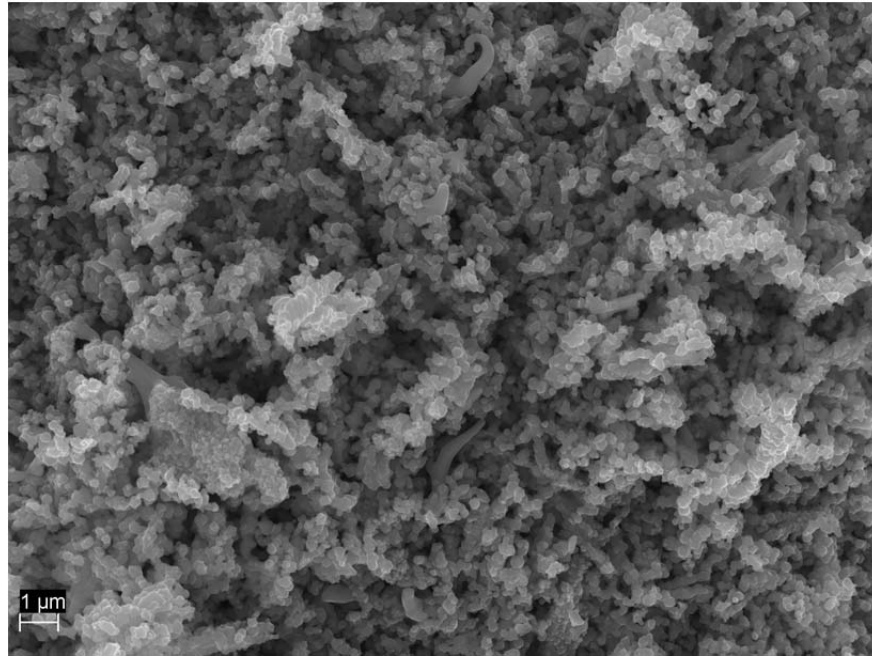
Figure 22.   Magnetite Partially Reduced by Coal and K_2CO_3 to FeO and Fe 5k Magnification
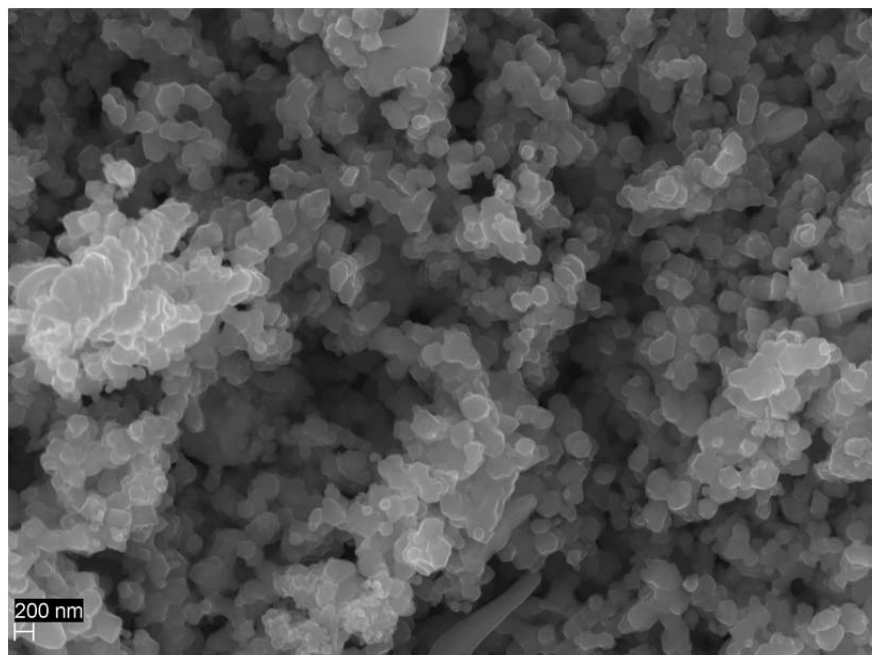
Figure 23. Magnetite Partially Reduced by Coal and K_2CO_3 to FeO and Fe 12.5k Magnification
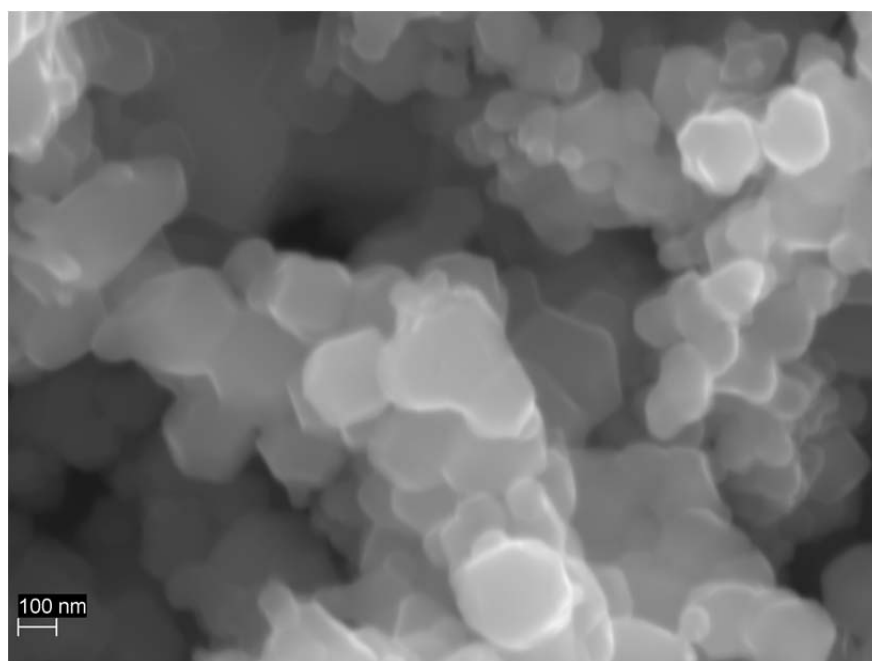
Figure 24. Magnetite Partially Reduced by Coal and K_2CO_3 to FeO and Fe 50k Magnification

The characteristics of the partially reduced FeO and Fe powder is very similar to that of the untreated magnetite, in that the high degree of regularity is clear. As observed from the nickel oxide experiments, the size of the particles does not appear to be impacted by the treatment process. This indicates that there has been no sintering of the particles at the operating temperatures used for this study.

THIS PAGE INTENTIONALLY LEFT BLANK

VI.   DISCUSSION

A.   DEMONSTRATING THE SHAR PROCESS

Overall the results demonstrate that the SHAR hypothesis is correct. To wit: Species generated via the thermal decomposition or volatilization of hydrocarbons can reduce metal oxides. In particular, it is clear from Figure 11 and Table 5 that NiO is fully and rapidly reduced at 850 °C by species evolved via the thermal decomposition of paraffin wax. This statement is based on the fact that there is no physical contact between the paraffin and the NiO at any time. There is a gap that can only be traversed by gas species, and these gas species must be produced by the thermal decomposition, or volatilization, of the hydrocarbon. The contrast with control experiments shown in Figures 9 and 10 makes this abundantly clear. No reduction is observed in the absence of the solid hydrocarbon. This in itself is an important and novel observation as generally reduction of solids is accomplished via gas phase species such as hydrogen or CO. That is, we have demonstrated a novel chemical process for a very significant industrial process, the reduction of oxides to metal. This process does bear some relationship to the process that takes place in a typical blast furnace, but is clearly distinct. Indeed, in blast furnace operation gas phase oxygen is required. No oxygen gas is employed in the SHAR process.

B.   FACTORS IMPACTING THE SHAR PROCESS

The results also demonstrate that many factors influence the efficacy of the process including the identity of the solid hydrocarbon, the presence of catalysts, and the identity of the metal oxide. An example of the influence of the first two parameters can be gleaned from an examination of the NiO results. Regarding the influence of hydrocarbon identity: Whereas NiO was totally reduced by the evolution of gas species from paraffin at a relatively low temperature, 850 C, it was only partially reduced by lignite under the same conditions, as shown in Table 10.

The influence of catalyst on NiO reduction can most clearly be observed in the contrast at 850 °C between the degree of NiO reduction with Na_2CO_3 catalyst (~76%) vs. the amount reduced in the presence of K_2CO_3 (~17%) under the same conditions. In fact the latter value is slightly less than the fractional reduction observed in the absence of catalyst. It appears that if anything K_2CO_3 has a negative impact on the reduction process when conducted at 850 C. However, the Na_2CO_3 reduction value suggests catalyst can play an important role in enhancing the efficacy of a very inexpensive form of solid hydrocarbon, lignite coal, for the SHAR process.

The fact that all the results show that under reducing conditions iron is more difficult to reduce than NiO shows that the SHAR process will work better with some oxides than others. This is not surprising as it is a long established fact, one quantifiably consistent with thermodynamics, some oxides are far more difficult to reduce than others. Still, it is valuable to contrast the results of SHAR reduction of nickel oxide with those of iron oxide. The primary contrast: magnetite (Fe_3O_4) was only partially reduced to wustite (FeO) under conditions that led to the complete reduction of NiO. Specifically, whereas NiO was fully, or almost fully reduced by paraffin or catalyst promoted paraffin at 850 C, under the same conditions no iron metal formed at all. The only reduced species observed was wustite, and the fraction of this species in the product was relatively small (~13%). Also, in the presence of coal, without catalyst, NiO was partially reduced (25%), but magnetite under identical conditions was not reduced at all.

Metallic iron was only found following the process in which coal was promoted with K_2CO_3 and the temperature employed was 950 °C rather than the standard 850 C. This does demonstrate that the SHAR process can be adapted to the reduction of iron ore, but the process as conducted in this initial investigation is far from adequate.

C.   SELECTION OF REDUCING SPECIES

Several reducing species were selected in order to demonstrate that the SHAR process is a general one. The present results clearly support, although do not prove, the hypothesis that any hydrocarbon which can be thermally decomposed or volatilizes can be used to reduce metal oxides using the SHAR process. Paraffin and wax from a candle were chosen as relatively generic sources of hydrocarbon. Lignite coal was selected as it represents a very inexpensive source of hydrocarbon. At the time of publishing, commodity prices for paraffin are in the range of $600 - $800 U.S. per ton, compared to $15 - $25 per ton for lignite. Coal is already the preferred source of hydrocarbons in industrial metal reduction processes and has a well-established production and distribution infrastructure. This combination of availability and cost effectiveness suggests the commercial viability of SHAR.

D.   SELECTION OF CATALYSTS

Catalysts that are well known to aid in coal combustion were selected for this study. Various studies in the literature regarding the mechanism of coal combustion catalysts suggest these catalysts greatly enhance the rate of volatile species production from coal. Indeed, as shown elsewhere [20], the mechanism of catalytic combustion of coal by alkali metals and carbonates, particularly K_2CO_3 and Na_2CO_3 roughly involve these steps. First, upon exposure to elevated temperatures the catalyst (e.g. K_2CO_3) wets the surface of the coal. That is, instead of forming particles of K_2CO_3, as is the general understanding of the morphology of heterogeneous catalysts, the coal catalyst forms a monolayer of partially oxidized potassium on the surface of the coal. It is important to note that this process takes place from a physical mixture of coal and catalyst. There is no need for a process to impregnate the coal with the catalyst. Second, an oxygen atom from the thin layer of the potassium oxide reacts with the carbon atoms in the coal, generally forming a volatile CO species. Third, upon exposure to gas phase oxygen, the original K-oxide surface phase reforms. This allows Step 2 to

recur. The oxidation / reduction cycle of the potassium carbonate catalyst takes place repeatedly until the coal is fully combusted.

The catalytic process for Na_2CO_3 is believed to be nearly the same as that described for potassium. However, there are differences. First, the thinly spread sodium phase is thought to be closer to metallic than is the case with potassium. Second, and more germane to the current work, is that the sodium coverage appears to decrease with temperature and the potassium to increase. The dispersion of the sodium on coal after a 900 °C treatment is about one-half that after a 500 °C treatment [21]. In contrast the potassium dispersion increases with temperature. The dispersion on coal after a 900 °C treatment is more than three times higher than it is after treatment at 500 °C [21]. This suggests that sodium might be a better low temperature combustion catalyst and potassium a better high temperature catalyst.

In the present study an excess of carbonate, either sodium or potassium, was physically mixed with the coal. It was postulated that oxygen atoms from carbonate molecules not participating in the thin surface catalyst phase makes up for oxygen at the carbonate/coal interface lost due to CO formation. This would permit the oxidation/reduction process to take place repeatedly. In this fashion coal could be a source of a volatile reducing species, carbon monoxide.

The results are qualitatively consistent with the postulated model. First, potassium carbonate (on lignite) did not seem to lead to any iron reduction at 850 C, whereas sodium carbonate (lignite) was a good catalyst for converting iron into wustite at this temperature. However, at 950 °C the coal treated with catalyst was most effective at iron reduction, actually allowing some metallic iron to form. In contrast the sodium catalyst only yielded wustite.

E.   THERMODYNAMIC ANALYSIS

In this work, it is clear that SHAR is an effective means of reducing nickel oxide and iron oxide to metal. Indeed, as demonstrated in Table 4, nickel oxide can be reduced by the thermal decomposition of paraffin in a bed under a bed of

nickel oxide powder. Iron oxide was more difficult to reduce, and in fact in this first study, only partial reduction was achieved. However, this partial reduction is believed to demonstrate the potential for full reduction.

This work also provides insight into the effectiveness of different solid hydrocarbons. Paraffin was found to be the most effective, but is also the most expensive, hydrocarbon employed. Coal, specifically low cost lignite coal, and catalyzed coal was less effective than paraffin, but far less costly, hence more likely to be used for further SHAR technique development.

To focus further development of the SHAR process and to attempt to understand the effectiveness disparity between nickel and iron oxides, the thermodynamics must be analyzed in detail.

For the purpose of this analysis, it is assumed that the reduction of the metal oxide powder is performed by carbon monoxide produced by the decomposition of the hydrocarbon source. This is a reasonable assumption, and is the same assumption made regarding the iron oxide reducing species created in coal reacting with air in a blast furnace. It is interesting to note that $CaCO_3$ (limestone) is also present in a blast furnace, mixed with the coal. It is reasonable to assume this material is actually a catalyst that provides oxygen atoms, rather than oxygen molecules, enabling the conversion of coal into CO. It is germane to this model to note neither calcium carbonate, nor any other alkali earth metals, is a quality coal gasification catalyst. In this regard it is relevant to note that coal gasification generally takes place at a temperature of less than 1000 C, whereas in a blast furnace the melting temperature of metallic iron (~1540 C) is reached. At these temperatures limestone may be an excellent catalyst.

Given the assumption that CO is the reducing species, the reduction of nickel oxide in this manner obeys Equation 7:

$$NiO + CO \rightarrow Ni + CO_2 \qquad (7)$$

The spontaneity of a chemical process can be determined by calculating the standard free energy change using Equation 8, where ΔG_f^o is the standard free energy of formation for each species in the reaction, and v is the coefficient for the species in the balanced reaction.

$$\Delta G^o = \sum v\Delta G_f^o(products) - \sum v\Delta G_f^o(reac\tan ts) \tag{8}$$

If the standard free energy change is negative, it will be spontaneous in the forward direction; if positive, the reaction is nonspontaneous and requires additional energy input to occur. Values for the standard free energy of formation of many materials have been tabulated in many places in the literature [22]. General guidance for this analytical process can be found in many standard chemistry texts, though [23] was the primary reference.

The reduction of nickel oxide is analyzed to determine the standard free energy change as follows.

$$\Delta G^o = v_{Ni}\Delta G_{f-Ni}^0 + v_{CO_2}\Delta G_{f-CO_2}^0 - v_{NiO}\Delta G_{f-NiO}^0 - v_{CO}\Delta G_{f-CO}^0 \tag{9}$$

$$\Delta G^0 = (0) + (1)(-94.260) - (1)(-51.7) - (1)(-32.808) \tag{10}$$

$$\Delta G^0 = -9.752 \text{ kcal/mol} \tag{11}$$

The tabulated standard free energy values are valid under the condition of 25 C, but it is the thermodynamics of the reaction at the operating temperature that is of interest. The free energy change of a reaction related to the standard change in free energy by Equation 12 [24].

$$\Delta G = \Delta G^o + RT\ln Q \tag{12}$$

In this equation, R is the ideal gas constant, T is absolute temperature, and Q is the reaction quotient. At equilibrium, Q is the equilibrium constant for the reaction, K_{eq}, and ΔG is zero. Equation 13 then simplifies to the familiar form in of Equation 13.

$$\Delta G^o = -RT\ln K_{eq} \tag{13}$$

This equation can then be solved for the equilibrium constant as shown in Equation 14.

$$K_{eq} = e^{-\Delta G^o/RT}$$
(14)

The equation is then evaluated for the operating temperature of 850 C.

$$K_{eq} = e^{-\Delta G^o/RT} = EXP\left[-9752\frac{cal}{mol}*\frac{1}{1.987}\frac{mol*K}{cal}*\frac{1}{(850+273.15)K}\right]$$
(15)

$$K_{eq} = 79.025$$
(16)

The equilibrium constant is often defined by the law of mass action [9], which will be demonstrated using a general equilibrium reaction as an example.

$$aA + bB \rightleftarrows cC + dD$$
(17)

In this case, A, B, C, and D are the species of the reaction, and a,, b, c, and d are the coefficients of the balanced reaction. The equilibrium constant is then found numerically by Equation 18, where the square brackets indicate molar concentration.

$$K_{eq} = \frac{[C]^c[D]^d}{[A]^a[B]^b}$$
(18)

The equilibrium condition for the nickel oxide reduction can be investigated using this equation. Assuming one mole of each reactant, the equilibrium state and gaseous constituents can be quantified by constructing a table describing the equilibrium state [25].

Table 16. Equilibrium Table: Nickel oxide reduction

Species	Initial Amount	Final Amount	Present in Gas Phase	Gas Phase Mole Fraction
NiO	1	1-X		
CO	1	1-X	1-X	(1-X)/1
Ni	0	X		
CO_2	0	X	X	X/1
Total			1	

The gaseous equilibrium constant defined by Equation 18 then simplifies to Equation 19.

$$K_{eq} = \frac{X}{1-X} \tag{19}$$

Rearranging this definition then yields the unknown X in Table 16.

$$X = \frac{K_{eq}}{1+K_{eq}} = \frac{79.025}{1+79.025} = 0.987 \tag{20}$$

This process shows that when a mole of carbon monoxide interacts with a mole of nickel oxide, most of the carbon monoxide converts to carbon dioxide via the process of removing oxygen from the solid oxide. Only one percent of the original CO produced (e.g. from volatilized lignite coal) remains in the gas phase to satisfy equilibrium.

The reduction of iron oxide is investigated using the same procedure. This chemical process follows Equation 21.

$$Fe_3O_4 + 4CO \rightarrow 3Fe + 4CO_2 \tag{21}$$
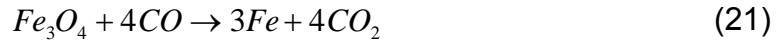
From this balanced reaction, the standard free energy change is determined to be -3.508 kcal/mol, and the equilibrium constant is calculated.

$$K_{eq} = e^{-\Delta G^o/RT} = EXP\left[-3508\frac{cal}{mol} * \frac{1}{1.987}\frac{mol*K}{cal} * \frac{1}{(850+273.15)K}\right] \tag{22}$$

$$K_{eq} = 4.815 \tag{23}$$

The equilibrium table, Table 17, is constructed. Once again a single mole of each reactant is assumed.

Table 17.   Equilibrium Table: Iron oxide reduction

Species	Initial Amount	Final Amount	Present in Gas Phase	Gas Phase Mole Fraction
Fe_3O_4	1	1-X		
CO	4	4-X	4-X	(4-X)/(4+3X)
Fe	0	3X		
CO_2	0	4X	4X	4X/(4+3X)
Total			4+3X	

The gas phase equilibrium then simplifies and evaluates to Equation 24.

$$K_{eq} = \frac{4X}{4-X} \tag{24}$$

Rearranging this definition then yields the unknown X in Table 17.

$$X = \frac{4K_{eq}}{4+K_{eq}} = \frac{4*4.815}{4+4.815} = 2.185 \tag{25}$$

Inserting this value of X into the expression for mole fraction in the gas phase reveals that at equilibrium, greater than 17 percent of the CO cannot be converted to CO_2 in order to maintain equilibrium. Stoichiometry also shows the need for 33 % more oxygen removal from Fe_3O_4, relative to NiO, to fully reduce one mole of iron. It is clear that the reduction of nickel oxide is more favored from a thermodynamic standpoint than iron oxide.

The analysis is valid for the operating temperature used for the initial experimental phase, but can easily be adapted to other temperatures, as all other

variables are either tabulated properties or the result of the balanced chemical reaction. The mole fraction of CO_2 in the gas phase is plotted in Figure 25 as a function of operating temperature. This corresponds to the percentage of CO that has been converted by the reduction of magnetite.
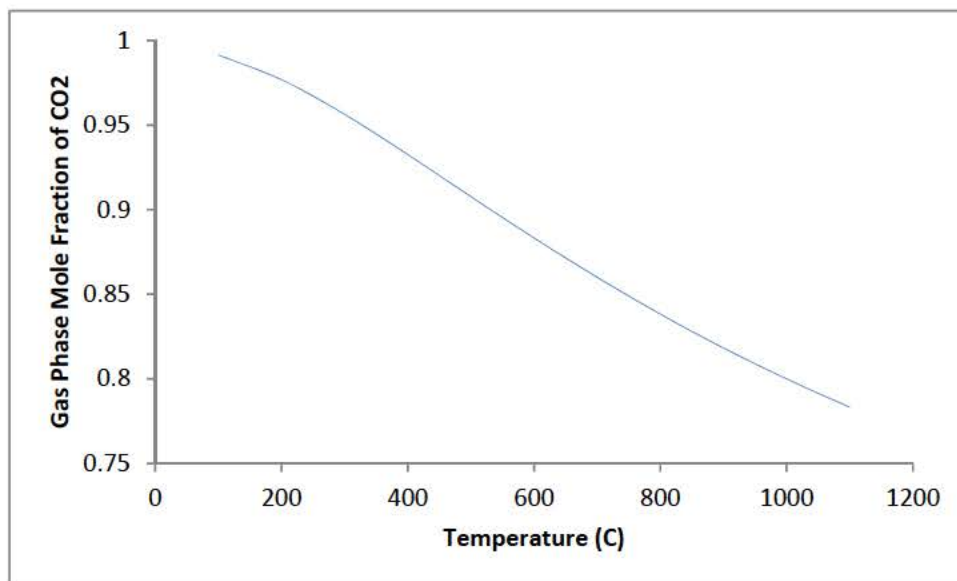

Figure 25.   Gas Phase Mole Fraction of CO_2

The limitation of this analysis is that the effect of temperature on the thermal and catalytic decomposition of the hydrocarbon source is not evaluated, and the thermal impacts on diffusion rates are ignored. The result is useful however, in that it illustrates that simply raising the operating temperature of the reaction is not the clear path toward improving the SHAR technique.

Another limitation of the present analysis is that it provides little insight into the rate or kinetics of the process. Thus, it is still not clear if the relative difficulty of reducing iron oxide vs. nickel oxide is thermodynamically or kinetically limited. Indeed, it is difficult to argue that thermodynamics is the only limiting factor. Most of the CO is available thermodynamically to reduce iron, yet reduction is far less than with NiO under the same conditions. Further study is required to determine the mechanism and the means to reach pure metallic iron using SHAR.

The study focused on the combination of materials used to determine the efficacy of the SHAR hypothesis. Time was not a primary variable of investigation, but may be of great importance for future research. Experiments utilizing solid hydrocarbons resulted in dramatically less residual material in the alumina vessel compared to that of the coal experiments. It was postulated that the high degree of reduction observed in paraffin experiments is related to the degree of decomposition of the carbon source. Indeed, a review of the literature revealed that paraffin decomposition by pyrolysis is exclusively a free radical process, rather than a molecular one [26]. This coupled with complete decomposition of the paraffin explains why the reduction process was completed to a great degree for these experiments.

By contrast, the pyrolysis of coal in the absence of catalysts results in a two-phase decomposition and degasification process. In the first phase, the coal softens, resulting in the release of primary gasses, consisting of carbon, oxygen, and hydrogen. The process then transitions to a hardening transition, commensurate with the release of secondary gas made primarily of hydrogen [27]. Additionally, the temperature at which coal is heat treat has a strong impact on the nature of the decomposition [28]. The highly dynamic nature of coal pyrolysis was not accounted for in the present study, and demands further inspection.

The addition of gasification catalysts to the coal adds oxygen to the process. That is, as discussed in the scientific literature, [20] among others, oxygen atoms from either the potassium or sodium carbonate catalysts interact with the carbon in coal to produce CO and other O-based radicals far more rapidly, and at lower temperature than is possible in the absence of catalyst. The present work shows that the effect on the SHAR process of carbonate catalyst addition to the coal is pronounced. In the absence of catalyst, there is very modest reduction of nickel and no iron reduction. The addition of catalyst to the lignite coal dramatically increases nickel reduction and leads to conversion of most of the iron to a lower reduction state.

The geometry of the experimental apparatus is not ideal in that the flow of nitrogen for atmosphere control is perpendicular to that required for hydrocarbon decomposition products to reach the target oxide. Ensuring greater interaction between these decomposition products and the metal oxide powder may be achieved by conducting experiments in a tube furnace of vertical orientation, or the construction of a vertically oriented containment that can be inserted in a bench top furnace.

While maintaining a similar sample arrangement of coal and catalyst mixture separated by stainless steel screen from the metal oxide in a vertical tube, the purge gas would force the gaseous pyrolysis products directly through the metal oxide. The vertical arrangement would eliminate the sample size limitation introduced by the volume of the alumina boat used in this study, creating freedom to optimize the mass ratio of oxide, coal and catalyst.

VII. CONCLUSION

This experiment was conducted to test the potential for the SHAR technique to reduce metal oxide powders, and promising results were obtained. Using gaseous products of hydrocarbon decomposition, complete reduction of nickel oxide powder was achieved. Partial reduction of iron oxide powder was also achieved, and there is reasonable expectation that the technique may be optimized to obtain complete reduction. This constitutes a novel approach to producing reduced metal particles in a way not currently in use in industry.

The low temperature and material requirements for the technique to be effective, as well as the batch nature of the process make it a prime candidate for as-needed manufacturing techniques that have the potential to dramatically impact the supply and logistic infrastructure for hard parts on board naval vessels. Reducing the storage requirements for such components in the fleet has the benefit of enabling the repurposing of existing storage spaces to house mission critical equipment such as sensors and armament. This directly impacts fleet readiness and mission effectiveness simultaneously.

Continued improvement and further study of the SHAR process is vital. Future studies should focus on improving the reduction of iron oxide via the SHAR method, but also on the reduction of alloying agents common in the steelmaking industry, such as chromium, manganese and cobalt. Improving the SHAR method for these oxides would open the possibility of using additive manufacturing techniques to produce alloy-based components, which quite simply could change the way the U.S. Navy does business.

THIS PAGE INTENTIONALLY LEFT BLANK

LIST OF REFERENCES

[1]   H. Toriya, 3D Manufacturing Innovation: Revolutionary Change in Japanese Manufacturing with Digital Data. Tokyo, Japan: Springer Science & Business Media, 2008.

[2]   U.S. House. 113th Congress, Committee on Small Business. (2014, Mar 12). *The rise of 3D printing: opportunities for entrepreneurs.* [Online]. Available: http://smallbusiness.house.gov/calendar/eventsingle.aspx?EventID= 364957

[3]   S. J. Freedberg. (2014, Apr. 22). Navy Warship Is Taking 3D Printer To Sea; Don't Expect A Revolution. [Online]. Available: http://breakingdefense.com/2014/04/navy-carrier-is-taking-3d-printer-to-sea-dont-expect-a-revolution/

[4]   Y. Tadjdeh. (2014, Oct.). Navy beefs up 3D printing efforts with new 'print the fleet' program. [Online]. Available: http://www.nationaldefensemagazine.org/archive/2014/October/Pages/NavyBeefsUp3DPrintingEffortsWithNewPrinttheFleetProgram.aspx

[5]   P. Cullom. (2014, Jul. 15). 5 things to know about Navy 3D printing. [Online]. Available: http://navylive.dodlive.mil/2014/07/15/5-things-to-know-about-navy-3d-printing/

[6]   R. M. German, "Progress in titanium metal powder injection molding," *Materials,* vol. 6, pp. 3641-3662, 2013.

[7]   J. González-Gutiérrez, G. B. Stringari and I. Emri, *Powder Injection Molding of Metal and Ceramic Parts.* INTECH Open Access Publisher, 2012.

[8]   K. Nishiyabu, *Micro Metal Powder Injection Molding.* INTECH Open Access Publisher, 2012.

[9]   T. Brown, H. LeMay and B. Bursten, *Chemistry: The Cetral Science.* Upper Saddle River, New Jersey: Pearson Education, 2003.

[10]   A. Cottrell, *An Introduction to Metallurgy.* Cambridge, England: Universities Press, 1975.

[11]   D. Proctor, K. Fehling, E. Shay, J. Wittenborn, J. Green, C. Avent, R. Bigham, M. Connolly, B. Lee and T. Shepker, "Physical and chemical characteristics of blast furnace, basic oxygen furnace, and electric arc

furnace steel industry slags," *Environ. Sci. Technol.,* vol. 34, pp. 1576-1582, 2000.

[12]   J. Kotz and P. Treichel, *Chemistry and Chemical Reactivity.* Fort Worth, Texas: Cengage Learning, 1999.

[13]   M. Popov, "Model experiments on atomization of liquids," *Acad. Rep. Populare Romane, Rev. De Mécanique Appliquee (Bucharest),* vol. 1, pp. 71, 1956.

[14]   G. B. Petrazhitskiy, "Experimental investigation of droplet vaporization under conditions of high temperaturs and pressures," *I. I. Mechnikova,* vol. 150, pp. 125, 1960.

[15]   J. Revilock, ""Grafoil"graphite tape: its manufacture properties, and uses," Am.Chem.Soc., Div.Fuel Chem., Prepr.;(United States), vol. 12, 1968.

[16]   B. L. Gabriel, *SEM: A User's Manual for Materials Science.* Metals Park, Ohio: 1985.

[17]   J. I. Goldstein, D. E. Newbury, P. Echlin, D. C. Joy, C. Fiori and E. Lifshin, *Scanning Electron Microscopy and X-Ray Microanalysis. A Text for Biologists, Materials Scientists, and Geologists.* New York: Plenum Publishing Corporation, 1981.

[18]   S. Amelinckx, *Modern Diffraction and Imaging Techniques in Material Science.* Amsterdam: North Holland Publishing Company, 1970.

[19]   C. Suryanarayana and M. G. Norton, *X-Ray Diffraction: A Practical Approach.* New York, New York: Plenum Press, 1998.

[20]   A. Gow and J. J. Phillips, "Microcalorimetric Study of Oxygen Adsorption on Catalytically Promoted Gassification Chars," *Journal of Catalysis,* vol. 132, pp. 388, 1991.

[21]   A. Gow and J. Phillips, "Microcalorimetric Study of Oxygen Adsorption on Catalytically Promoted Gasification Chars: Mechanistic Evidence for Alkali- and Alkaline-Earth-Metal Carbonate Catalyzed Reactions," *Energy & Fuels,* vol. 6, pp. 526, 1992.

[22]   W. M. Haynes, CRC Handbook of Chemistry and Physics. Boca Raton, Florida: CRC press, 2013.

[23]   S. Sandler, *Chemical and Engineering Thermodynamics.* New York, New York: John Wiley & Sons, 1989.

[24]   C. E. Reid, *Principles of Chemical Thermodynamics.* London, England: Reinhold, 1960.

[25]   K. Denbigh, *The Principles of Chemical Equilibrium.* Cambridge, England: Cambridge University Press, 1966.

[26]   P. G. Ashmore, T. Sugden and F. Dainton, *Photochemistry and Reaction Kinetics.* Cambridge, England: Cambridge University Press, 1967.

[27]   D. W. Van Krevelen and J. Schuyer, *Coal Science: Aspects of Coal Constitution.* Amsterdam: Elsevier, 1957.

[28]   A. Gow and J. Phillips, "Microcalorimetric Study of Reactive Surface Area on Demineralized Coal Chars," *Energy & Fuels,* vol. 7, pp. 674, 1993.

THIS PAGE INTENTIONALLY LEFT BLANK

INITIAL DISTRIBUTION LIST

1. Defense Technical Information Center
   Ft. Belvoir, Virginia

2. Dudley Knox Library
   Naval Postgraduate School
   Monterey, California